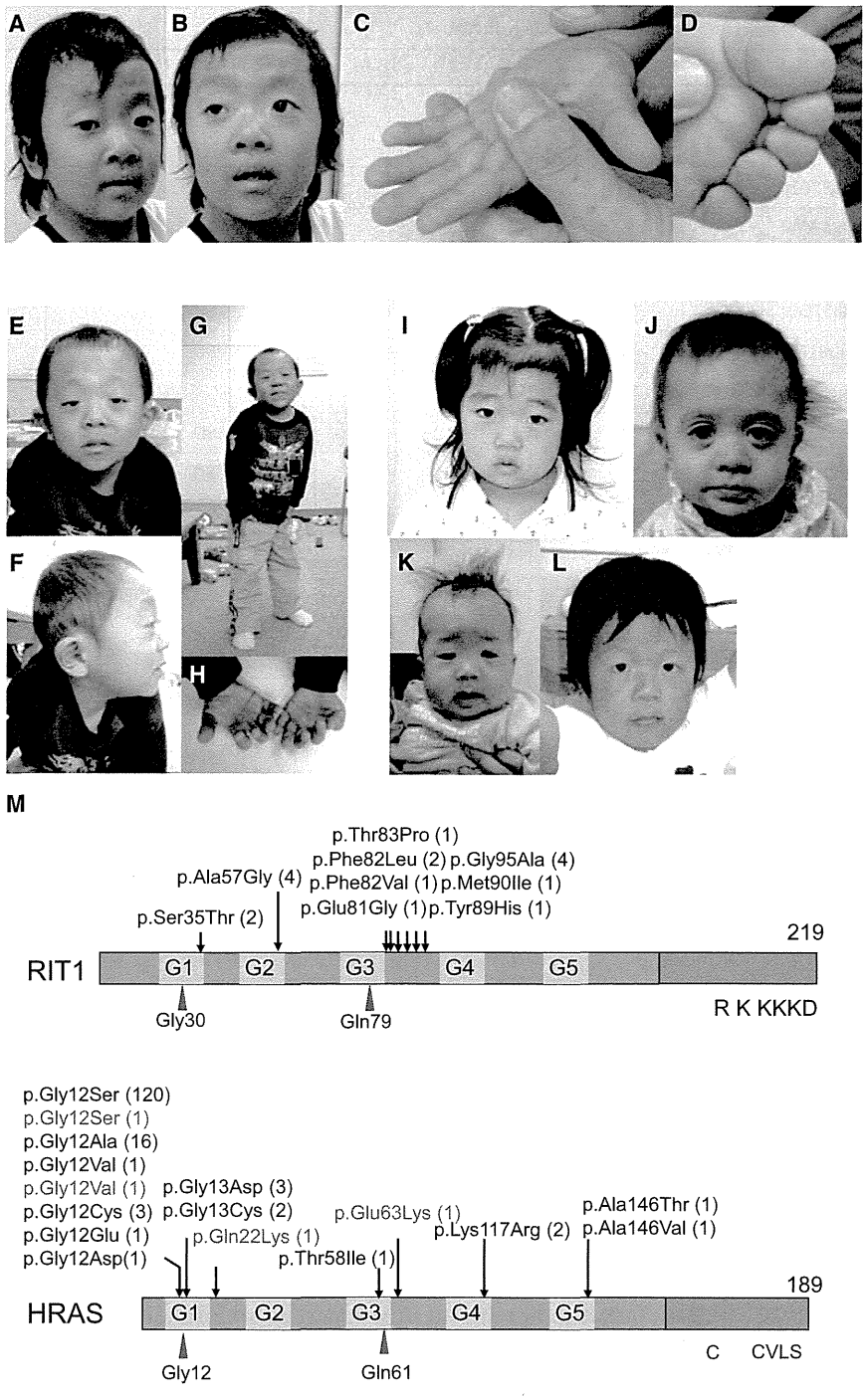

Figure 1. Photographs of Six Individuals in whom *RIT1* Mutations Were Identified
(A–D) KCC38 at 3 years of age. Broad forehead, sparse eyebrows, ptosis, hypertelorism, and hyperpigmentation were observed (A and B). Prominent finger pads were observed (C and D).
(E–H) NS358 at 4 years of age. Hypertelorism, epicanthus, sparse eyebrows, and low-set ears were observed.
(I) NS414 at 3 years of age.
(J) NS465 at 1 year of age.
(K) NS276 at 5 months.
(L) NS265 at 5 years of age.
(M) Structure and identified germline alterations in RIT1 and HRAS. HRAS alterations identified in individuals with Costello syndrome were described before[20] or shown in The RAS/MAPK Syndromes Homepage (see Web Resources). HRAS alterations identified in individuals with congenital myopathy with excess of muscle spindles[35] are indicated in purple.
We obtained specific consent for photographs from six individuals.

in 125/132 (94.7%) embryos; however, 7/132 (5.3%) embryos had limited mild craniofacial and heart abnormalities (Table 2). In contrast, a combined manifestation of craniofacial abnormalities, pericardial edema, and an elongated yolk sac was observed in 66.1%, 52.4%, and 40.5% of embryos expressing p.Gln79Leu, p.Glu81Gly, and p.Gly95Ala, respectively. Development was severely retarded in approximately 7% of embryos expressing RIT1 alterations; these embryos displayed the formation of a disorganized round body shape with a dysmorphic head and body trunk. In the head region, a hypoplastic brain, especially in the telencephalic area, was observed and resulted in misshapen morphology. In the ventral part of the head, the jaw structure was also hypoplastic, and the eyes were translocated medially. These morphological changes gave a cyclopia-like appearance. The ventral sides of the eyes were small, and coloboma along with a loss of pigment was evident (Figure 3B). These phenotypic changes are compatible with the gastrulation defect observed at 11 hpf (Figure 3A). Because the Fgf/Ras/MAPK signaling cascade plays an essential role in the convergent and extension cell movement during gastrulation,[41] perturbation by the RIT1 alterations could cause abnormal cell movement in the axial portions and thus lead to an elongated shape of the egg and the hypoplastic ventral side of the head. Detailed inspection of the morphology in mutant-injected embryos revealed abnormal cardiogenesis, namely, incomplete looping, hypoplastic chambers, and stagnation of blood flow in the yolk sac (Figure 3B). Although the atrium of these hearts beat regularly, the ventricle seemed to twitch passively by the contraction of the atrium (Movies S1, S2, S3, S4, S5, and S6). These results indicate that activating mutations in *RIT1* induce abnormal craniofacial and heart defects in zebrafish.

RIT1-mutation-positive individuals showed a distinct facial appearance, congenital heart defects, and skeletal

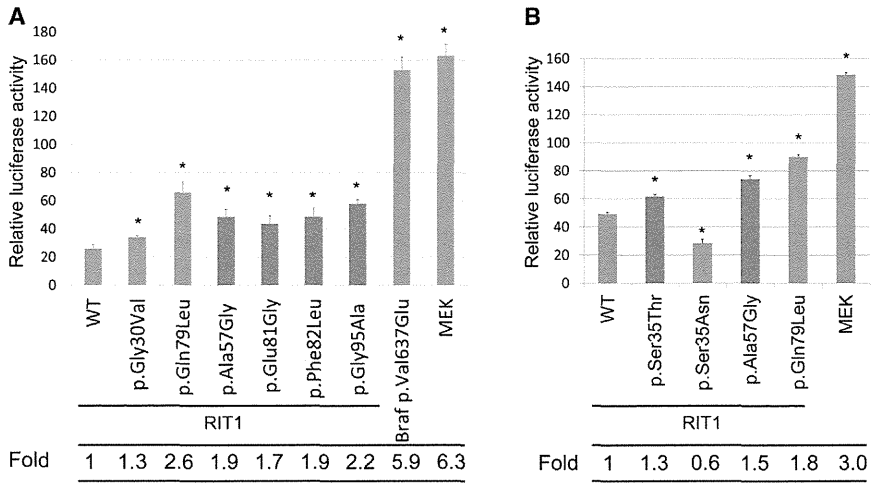

Figure 2. Stimulation of ELK Transcription in NIH 3T3 Cells Expressing *RIT1* Germline Mutations

(A) The ELK1-GAL4 vector and the GAL4 luciferase *trans*-reporter vector were transiently transfected with various *RIT1* germline mutations and activating mutations in *BRAF* and *MAP2K1* in NIH 3T3 cells. c.1910T>A (p.Val637Glu) in mouse *Braf* corresponds to oncogenic c.1799T>A (p.Val600Glu) in human *BRAF*. Relative luciferase activity was calculated by normalization to the activity of a cotransfected control vector, phRLnull-luc, containing distinguishable *R. reniformis* luciferase.

(B) ELK1 transactivation in cells expressing p.Ser35Thr, identified in individuals with Noonan syndrome, and p.Ser35Asn, were examined. p.Ser35Asn corresponds to dominant-negative alteration p.Ser17Asn in RAS.

Results are expressed as the means of quadruplicate (A) and triplicate (B) samples. Error bars represent the SDs of mean values. Red bars indicate germline *RIT1* mutations identified in Noonan syndrome. The following abbreviation is used: WT, wild-type. *$p < 0.01$ by t test.

abnormalities and were diagnosed with Noonan syndrome by diagnostic criteria developed by van der Burgt (Figures 1A–1L and Table 1).[4] Two individuals (NS358 and KCC38) were suspected to have CFC syndrome in the infantile period because of curly, sparse hair, a high cranial vault, and hypoplasia of the supraorbital ridges. Nine individuals showed perinatal abnormality, including polyhydramnios, nuchal translucency, and chylothorax (Table S2). It is of note that one individual (Og45) showing severe pleural effusion, hypertrophic cardiomyopathy, and hepatomegaly that ended in severe body edema and compromised circulation died 53 days after birth. Seven individuals showed high birth weight, probably as a result of subcutaneous edema, which is a typical manifestation observed in individuals with Noonan syndrome.[4] Out of 17 affected individuals, 16 (94%) had heart defects (Table 1): hypertrophic cardiomyopathy (HCM) in 12 (71%) individuals, pulmonary stenosis in 11 (65%) individuals, and atrial septal defects in 5 (29%) individuals. The incidence of pulmonic stenosis and mild cognitive defects is close to the overall incidence of these features in Noonan syndrome cohorts. By contrast, the incidence of HCM is far greater than in individuals with Noonan syndrome overall (25/118 in Noonan syndrome[42] versus 12/17 in individuals with *RIT1* mutations; $p < 0.0001$ by Fisher's exact test). It is of note that a high frequency of HCM (70%) was also reported in individuals with *RAF1* mutations.[10,11,24] It is possible that RIT1 interacts with RAF1 and that gain-of-function mutations in *RIT1* and *RAF1* exert similar effects in heart development.

Somatic alterations in classical RAS have been identified in approximately 30% of tumors.[43] Noonan syndrome and related disorders confer an increased risk of developing malignant tumors.[20,44] In a summary of the literature, it has been reported that 45 of 1,151 (3.9%) individuals with Noonan syndrome (but with an unknown mutation status) developed malignant tumors.[44] Since molecular analysis became available, gene-specific association with malignant tumors has been revealed. The association with JMML, a myeloproliferative disorder characterized by the excessive production of myelomonocytic cells, has been reported in individuals with *PTPN11*, *CBL*, and *KRAS* mutations. Recent reports showed that two individuals with *SOS1* mutations developed embryonal rhabdomyosarcoma.[45,46] A somatic *RIT1* variant, c.270G>A (p.Met90Ile), has been identified in lung cancer (COSMIC database). In the present cohort, 1 (NS168) of 17 individuals with *RIT1* c.242A>G (p.Glu81Gly) developed acute lymphoblastic leukemia at the age of 5 years. The child was treated by a standard protocol and has remained in complete remission. Examining whether gain-of-function mutations in *RIT1* cause tumorigenesis will require further study.

RIT1 has been isolated as a cDNA encoding highly conserved G3 and G4 domains of RAS proteins[33] or identified as a gene encoding a protein related to *Drosophila Ric*, a calmodulin-binding RAS-related GTPase.[34] RIT1 p.Gln79Leu, which corresponds to RAS p.Gln61Leu, is implicated in transforming NIH 3T3 cells, neurite outgrowth in neuronal cells, and the activation of ERK and p38 MAPK in a cell-specific manner.[37,38,47] In this study, enhanced ELK1 transactivation was observed in cells expressing mutant *RIT1* cDNAs. Previous studies showed that enhanced ELK transactivation was observed in NIH 3T3 cells expressing *HRAS*, *KRAS*, *BRAF*, and *RAF1* mutations identified in individuals with Costello, CFC, and Noonan syndromes.[17,18,24] Gastrulation defects observed in zebrafish embryos expressing RIT1 alterations (p.Glu81Gly, p.Gly95Ala, or p.Gln79Leu) were also reported in zebrafish embryos expressing an activating mutation in *NRAS*, *BRAF*, *MAP2K1*, or *MAP2K2*.[40,48] Taken together, these

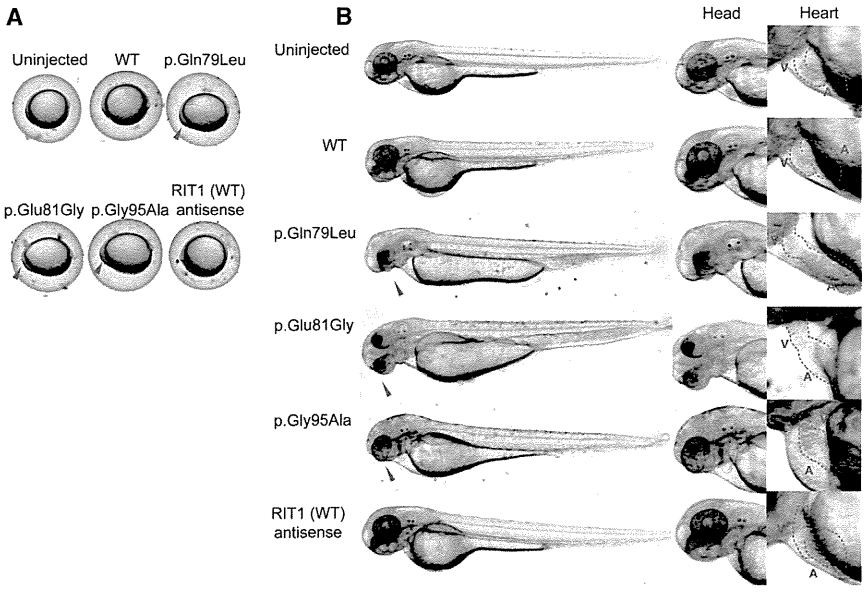

Figure 3. Morphology of Embryos Injected with the WT or Mutant *RIT1* mRNA

In vitro transcription of each mRNA was performed with the mMESSAGE mMACHINE kit (Applied Biosystems) according to the manufacturer's instructions. Synthesized mRNAs were purified with G-50 Micro Columns (GE Healthcare) and subsequently adjusted to a 300 ng/μl concentration for microinjection. Approximately 1 nl (300 pg) of RNA in water with 0.2% phenol red was injected into the cytoplasm of 1-cell-stage zebrafish embryos. Injected embryos were incubated at 28°C until observation.

(A) At 11 hpf, the shapes of the embryos injected with the WT sense or antisense mRNA were round, a normal morphology as observed in the uninjected embryos. In contrast, embryos expressing mutations (c.236A>T [p.Gln79Leu], c.242A>G [p.Glu81Gly], and c.284G>C [p.Gly95Ala]) are oval and compressed along the dorsal-ventral axis, indicative of a gastrulation defect. Note that cells have a hump in the head region at the anterior end of the body axis, the earliest manifestation of a craniofacial defect.

(B) Lateral views at 48 hpf are shown. Embryos expressing mutations (c.236A>T [p.Gln79Leu], c.242A>G [p.Glu81Gly], and c.284G>C [p.Gly95Ala]) formed swollen yolk sacs equally along the anterior posterior axis but did not show narrowing in the caudal half, which was clearly visible in the uninjected embryos and in those injected with the WT sense or antisense mRNA. In the craniofacial area, misshapen head and jaw structures and small eyes with hypoplasia on the ventral side were observed (middle panel); these phenotypes are consistent with the gastrulation defect. Shapes of the hearts (highlighted by red dotted lines) are shown in the right panel at a higher magnification. Normal looping of the heart tube and correct formation of two distinct chambers are observed in embryos injected with the WT sense or antisense mRNA. When mutations (c.236A>T [p.Gln79Leu], c.242A>G [p.Glu81Gly], and c.284G>C [p.Gly95Ala]) were expressed, looping was incomplete, resulting in stretched straight heart tubes. Constrictions at the atrial-ventricular canal are obscure, and the heart chambers are hypoplastic. Abbreviations are as follows: A, atrium; and V, ventricle.

results indicate that gain-of-function mutations in *RIT1* cause Noonan syndrome and show a similar effect to mutations in other RASopathy-related genes in human development.

Herein, we used whole-exome sequencing to identify germline *RIT1* mutations in individuals with Noonan syndrome, a disorder of the RASopathies. Mutations in *PTPN11*, *SOS1*, *RAF1*, *KRAS*, *BRAF*, and *NRAS* have been identified in 41%, 11%, 5%, 1%, 0.8%, and 0.2% of all cases, respectively,[3] and thus the frequency of *RIT1* mutations in Noonan syndrome might be similar to that of *RAF1* mutations. Our findings will improve diagnostic accuracy of Noonan syndrome and provide a clue to understanding the disorder's pathogenesis, including therapeutic approaches.

Supplemental Data

Supplemental Data include four figures, three tables, and six movies and can be found with this article online at http://www.cell.com/AJHG/.

Acknowledgments

The authors thank the families and the doctors who participated in this study. We are grateful to Jun-ichi Miyazaki at Osaka University for supplying the pCAGGS expression vector. We thank Yoko Narumi, Tomoko Kobayashi, Shoko Komatsuzaki, Yu Abe, Yuka Saito, Rumiko Izumi, Mitsuji Moriya, and Masako Yaoita for contributing to routine diagnostic work and Yoko Tateda, Kumi Kato, and Riyo Takahashi for their technical assistance. We are grateful to Eric Haan for sending samples of Noonan syndrome

Table 2. Morphologic Abnormality at 48–52 hpf of Zebrafish Embryos Injected with WT or Mutant RNA at the 1-Cell Stage

	No Abnormalities	Heart and Facial Abnormalities[a]	Severely Disorganized[b]	Total Number of Embryos
WT	125	7 (5.3%)	0 (0%)	132
p.Gln79Leu	31	78 (66.1%)	9 (7.6%)	118
p.Glu81Gly	42	55 (52.4%)	8 (7.6%)	105
p.Gly95Ala	44	34 (40.5%)	6 (7.1%)	84

[a]Craniofacial abnormalities, pericardial heart edema, and an elongated yolk sac were observed.
[b]Disorganized round body shape with a dysmorphic head and body trunk as shown in Figure S4.

and related disorders. We also acknowledge the support of the Biomedical Research Core of Tohoku University Graduate School of Medicine. This work was supported by the Funding Program for the Next Generation of World-Leading Researchers (NEXT Program) from the Ministry of Education, Culture, Sports, Science, and Technology of Japan (MEXT) to Y.A. (LS004), by Grants-in-Aids from MEXT, from the Japan Society for the Promotion of Science, and from the Ministry of Health, Labor, and Welfare to Y.M. and T.N. This work was supported in part by the National Cancer Center Research and Development Fund (23-22-11).

Received: April 23, 2013
Revised: May 19, 2013
Accepted: May 23, 2013
Published: June 20, 2013

Web Resources

The URLs for data presented herein are as follows:

Catalogue of Somatic Mutations in Cancer (COSMIC), http://www.sanger.ac.uk/genetics/CGP/cosmic/

Online Mendelian Inheritance in Man (OMIM), http://www.omim.org

RefSeq, http://www.ncbi.nlm.nih.gov/RefSeq

The RAS/MAPK Syndromes Homepage, http://www.medgen.med.tohoku.ac.jp/RasMapk%20syndromes.html

References

1. Takai, Y., Sasaki, T., and Matozaki, T. (2001). Small GTP-binding proteins. Physiol. Rev. *81*, 153–208.
2. Giehl, K. (2005). Oncogenic Ras in tumour progression and metastasis. Biol. Chem. *386*, 193–205.
3. Romano, A.A., Allanson, J.E., Dahlgren, J., Gelb, B.D., Hall, B., Pierpont, M.E., Roberts, A.E., Robinson, W., Takemoto, C.M., and Noonan, J.A. (2010). Noonan syndrome: clinical features, diagnosis, and management guidelines. Pediatrics *126*, 746–759.
4. van der Burgt, I. (2007). Noonan syndrome. Orphanet J. Rare Dis. *2*, 4.
5. Tartaglia, M., Mehler, E.L., Goldberg, R., Zampino, G., Brunner, H.G., Kremer, H., van der Burgt, I., Crosby, A.H., Ion, A., Jeffery, S., et al. (2001). Mutations in PTPN11, encoding the protein tyrosine phosphatase SHP-2, cause Noonan syndrome. Nat. Genet. *29*, 465–468.
6. Digilio, M.C., Conti, E., Sarkozy, A., Mingarelli, R., Dottorini, T., Marino, B., Pizzuti, A., and Dallapiccola, B. (2002). Grouping of multiple-lentigines/LEOPARD and Noonan syndromes on the PTPN11 gene. Am. J. Hum. Genet. *71*, 389–394.
7. Schubbert, S., Zenker, M., Rowe, S.L., Böll, S., Klein, C., Bollag, G., van der Burgt, I., Musante, L., Kalscheuer, V., Wehner, L.E., et al. (2006). Germline KRAS mutations cause Noonan syndrome. Nat. Genet. *38*, 331–336.
8. Roberts, A.E., Araki, T., Swanson, K.D., Montgomery, K.T., Schiripo, T.A., Joshi, V.A., Li, L., Yassin, Y., Tamburino, A.M., Neel, B.G., and Kucherlapati, R.S. (2007). Germline gain-of-function mutations in SOS1 cause Noonan syndrome. Nat. Genet. *39*, 70–74.
9. Tartaglia, M., Pennacchio, L.A., Zhao, C., Yadav, K.K., Fodale, V., Sarkozy, A., Pandit, B., Oishi, K., Martinelli, S., Schackwitz, W., et al. (2007). Gain-of-function SOS1 mutations cause a distinctive form of Noonan syndrome. Nat. Genet. *39*, 75–79.
10. Pandit, B., Sarkozy, A., Pennacchio, L.A., Carta, C., Oishi, K., Martinelli, S., Pogna, E.A., Schackwitz, W., Ustaszewska, A., Landstrom, A., et al. (2007). Gain-of-function RAF1 mutations cause Noonan and LEOPARD syndromes with hypertrophic cardiomyopathy. Nat. Genet. *39*, 1007–1012.
11. Razzaque, M.A., Nishizawa, T., Komoike, Y., Yagi, H., Furutani, M., Amo, R., Kamisago, M., Momma, K., Katayama, H., Nakagawa, M., et al. (2007). Germline gain-of-function mutations in RAF1 cause Noonan syndrome. Nat. Genet. *39*, 1013–1017.
12. Cirstea, I.C., Kutsche, K., Dvorsky, R., Gremer, L., Carta, C., Horn, D., Roberts, A.E., Lepri, F., Merbitz-Zahradnik, T., König, R., et al. (2010). A restricted spectrum of NRAS mutations causes Noonan syndrome. Nat. Genet. *42*, 27–29.
13. Cordeddu, V., Di Schiavi, E., Pennacchio, L.A., Ma'ayan, A., Sarkozy, A., Fodale, V., Cecchetti, S., Cardinale, A., Martin, J., Schackwitz, W., et al. (2009). Mutation of SHOC2 promotes aberrant protein N-myristoylation and causes Noonan-like syndrome with loose anagen hair. Nat. Genet. *41*, 1022–1026.
14. Loh, M.L., Sakai, D.S., Flotho, C., Kang, M., Fliegauf, M., Archambeault, S., Mullighan, C.G., Chen, L., Bergstraesser, E., Bueso-Ramos, C.E., et al. (2009). Mutations in CBL occur frequently in juvenile myelomonocytic leukemia. Blood *114*, 1859–1863.
15. Niemeyer, C.M., Kang, M.W., Shin, D.H., Furlan, I., Erlacher, M., Bunin, N.J., Bunda, S., Finklestein, J.Z., Sakamoto, K.M., Gorr, T.A., et al. (2010). Germline CBL mutations cause developmental abnormalities and predispose to juvenile myelomonocytic leukemia. Nat. Genet. *42*, 794–800.
16. Pérez, B., Mechinaud, F., Galambrun, C., Ben Romdhane, N., Isidor, B., Philip, N., Derain-Court, J., Cassinat, B., Lachenaud, J., Kaltenbach, S., et al. (2010). Germline mutations of the CBL gene define a new genetic syndrome with predisposition to juvenile myelomonocytic leukaemia. J. Med. Genet. *47*, 686–691.
17. Aoki, Y., Niihori, T., Kawame, H., Kurosawa, K., Ohashi, H., Tanaka, Y., Filocamo, M., Kato, K., Suzuki, Y., Kure, S., and Matsubara, Y. (2005). Germline mutations in HRAS proto-oncogene cause Costello syndrome. Nat. Genet. *37*, 1038–1040.
18. Niihori, T., Aoki, Y., Narumi, Y., Neri, G., Cavé, H., Verloes, A., Okamoto, N., Hennekam, R.C., Gillessen-Kaesbach, G., Wieczorek, D., et al. (2006). Germline KRAS and BRAF mutations in cardio-facio-cutaneous syndrome. Nat. Genet. *38*, 294–296.
19. Rodriguez-Viciana, P., Tetsu, O., Tidyman, W.E., Estep, A.L., Conger, B.A., Cruz, M.S., McCormick, F., and Rauen, K.A. (2006). Germline mutations in genes within the MAPK pathway cause cardio-facio-cutaneous syndrome. Science *311*, 1287–1290.
20. Aoki, Y., Niihori, T., Narumi, Y., Kure, S., and Matsubara, Y. (2008). The RAS/MAPK syndromes: novel roles of the RAS pathway in human genetic disorders. Hum. Mutat. *29*, 992–1006.
21. Tidyman, W.E., and Rauen, K.A. (2009). The RASopathies: developmental syndromes of Ras/MAPK pathway dysregulation. Curr. Opin. Genet. Dev. *19*, 230–236.
22. Groesser, L., Herschberger, E., Ruetten, A., Ruivenkamp, C., Lopriore, E., Zutt, M., Langmann, T., Singer, S., Klingseisen, L., Schneider-Brachert, W., et al. (2012). Postzygotic HRAS and KRAS mutations cause nevus sebaceous and Schimmelpenning syndrome. Nat. Genet. *44*, 783–787.

23. Abe, Y., Aoki, Y., Kuriyama, S., Kawame, H., Okamoto, N., Kurosawa, K., Ohashi, H., Mizuno, S., Ogata, T., Kure, S., et al.; Costello and CFC syndrome study group in Japan. (2012). Prevalence and clinical features of Costello syndrome and cardio-facio-cutaneous syndrome in Japan: findings from a nationwide epidemiological survey. Am. J. Med. Genet. A. *158A*, 1083–1094.
24. Kobayashi, T., Aoki, Y., Niihori, T., Cavé, H., Verloes, A., Okamoto, N., Kawame, H., Fujiwara, I., Takada, F., Ohata, T., et al. (2010). Molecular and clinical analysis of RAF1 in Noonan syndrome and related disorders: dephosphorylation of serine 259 as the essential mechanism for mutant activation. Hum. Mutat. *31*, 284–294.
25. Komatsuzaki, S., Aoki, Y., Niihori, T., Okamoto, N., Hennekam, R.C., Hopman, S., Ohashi, H., Mizuno, S., Watanabe, Y., Kamasaki, H., et al. (2010). Mutation analysis of the SHOC2 gene in Noonan-like syndrome and in hematologic malignancies. J. Hum. Genet. *55*, 801–809.
26. Narumi, Y., Aoki, Y., Niihori, T., Neri, G., Cavé, H., Verloes, A., Nava, C., Kavamura, M.I., Okamoto, N., Kurosawa, K., et al. (2007). Molecular and clinical characterization of cardio-facio-cutaneous (CFC) syndrome: overlapping clinical manifestations with Costello syndrome. Am. J. Med. Genet. A. *143A*, 799–807.
27. Narumi, Y., Aoki, Y., Niihori, T., Sakurai, M., Cavé, H., Verloes, A., Nishio, K., Ohashi, H., Kurosawa, K., Okamoto, N., et al. (2008). Clinical manifestations in patients with SOS1 mutations range from Noonan syndrome to CFC syndrome. J. Hum. Genet. *53*, 834–841.
28. Niihori, T., Aoki, Y., Okamoto, N., Kurosawa, K., Ohashi, H., Mizuno, S., Kawame, H., Inazawa, J., Ohura, T., Arai, H., et al. (2011). HRAS mutants identified in Costello syndrome patients can induce cellular senescence: possible implications for the pathogenesis of Costello syndrome. J. Hum. Genet. *56*, 707–715.
29. Saito, Y., Aoki, Y., Muramatsu, H., Makishima, H., Maciejewski, J.P., Imaizumi, M., Rikiishi, T., Sasahara, Y., Kure, S., Niihori, T., et al. (2012). Casitas B-cell lymphoma mutation in childhood T-cell acute lymphoblastic leukemia. Leuk. Res. *36*, 1009–1015.
30. Li, H., and Durbin, R. (2009). Fast and accurate short read alignment with Burrows-Wheeler transform. Bioinformatics *25*, 1754–1760.
31. McKenna, A., Hanna, M., Banks, E., Sivachenko, A., Cibulskis, K., Kernytsky, A., Garimella, K., Altshuler, D., Gabriel, S., Daly, M., and DePristo, M.A. (2010). The Genome Analysis Toolkit: a MapReduce framework for analyzing next-generation DNA sequencing data. Genome Res. *20*, 1297–1303.
32. Wang, K., Li, M., and Hakonarson, H. (2010). ANNOVAR: functional annotation of genetic variants from high-throughput sequencing data. Nucleic Acids Res. *38*, e164.
33. Lee, C.H., Della, N.G., Chew, C.E., and Zack, D.J. (1996). Rin, a neuron-specific and calmodulin-binding small G-protein, and Rit define a novel subfamily of ras proteins. J. Neurosci. *16*, 6784–6794.
34. Wes, P.D., Yu, M., and Montell, C. (1996). RIC, a calmodulin-binding Ras-like GTPase. EMBO J. *15*, 5839–5848.
35. van der Burgt, I., Kupsky, W., Stassou, S., Nadroo, A., Barroso, C., Diem, A., Kratz, C.P., Dvorsky, R., Ahmadian, M.R., and Zenker, M. (2007). Myopathy caused by HRAS germline mutations: implications for disturbed myogenic differentiation in the presence of constitutive HRas activation. J. Med. Genet. *44*, 459–462.
36. Niwa, H., Yamamura, K., and Miyazaki, J. (1991). Efficient selection for high-expression transfectants with a novel eukaryotic vector. Gene *108*, 193–199.
37. Rusyn, E.V., Reynolds, E.R., Shao, H., Grana, T.M., Chan, T.O., Andres, D.A., and Cox, A.D. (2000). Rit, a non-lipid-modified Ras-related protein, transforms NIH3T3 cells without activating the ERK, JNK, p38 MAPK or PI3K/Akt pathways. Oncogene *19*, 4685–4694.
38. Shi, G.X., and Andres, D.A. (2005). Rit contributes to nerve growth factor-induced neuronal differentiation via activation of B-Raf-extracellular signal-regulated kinase and p38 mitogen-activated protein kinase cascades. Mol. Cell. Biol. *25*, 830–846.
39. Cai, W., Rudolph, J.L., Harrison, S.M., Jin, L., Frantz, A.L., Harrison, D.A., and Andres, D.A. (2011). An evolutionarily conserved Rit GTPase-p38 MAPK signaling pathway mediates oxidative stress resistance. Mol. Biol. Cell *22*, 3231–3241.
40. Runtuwene, V., van Eekelen, M., Overvoorde, J., Rehmann, H., Yntema, H.G., Nillesen, W.M., van Haeringen, A., van der Burgt, I., Burgering, B., and den Hertog, J. (2011). Noonan syndrome gain-of-function mutations in NRAS cause zebrafish gastrulation defects. Dis Model Mech *4*, 393–399.
41. Fürthauer, M., Van Celst, J., Thisse, C., and Thisse, B. (2004). Fgf signalling controls the dorsoventral patterning of the zebrafish embryo. Development *131*, 2853–2864.
42. Burch, M., Sharland, M., Shinebourne, E., Smith, G., Patton, M., and McKenna, W. (1993). Cardiologic abnormalities in Noonan syndrome: phenotypic diagnosis and echocardiographic assessment of 118 patients. J. Am. Coll. Cardiol. *22*, 1189–1192.
43. Schubbert, S., Shannon, K., and Bollag, G. (2007). Hyperactive Ras in developmental disorders and cancer. Nat. Rev. Cancer *7*, 295–308.
44. Kratz, C.P., Rapisuwon, S., Reed, H., Hasle, H., and Rosenberg, P.S. (2011). Cancer in Noonan, Costello, cardiofaciocutaneous and LEOPARD syndromes. Am. J. Med. Genet. C. Semin. Med. Genet. *157*, 83–89.
45. Denayer, E., Devriendt, K., de Ravel, T., Van Buggenhout, G., Smeets, E., Francois, I., Sznajer, Y., Craen, M., Leventopoulos, G., Mutesa, L., et al. (2010). Tumor spectrum in children with Noonan syndrome and SOS1 or RAF1 mutations. Genes Chromosomes Cancer *49*, 242–252.
46. Jongmans, M.C.J., Hoogerbrugge, P.M., Hilkens, L., Flucke, U., van der Burgt, I., Noordam, K., Ruiterkamp-Versteeg, M., Yntema, H.G., Nillesen, W.M., Ligtenberg, M.J.L., et al. (2010). Noonan syndrome, the SOS1 gene and embryonal rhabdomyosarcoma. Genes Chromosomes Cancer *49*, 635–641.
47. Hynds, D.L., Spencer, M.L., Andres, D.A., and Snow, D.M. (2003). Rit promotes MEK-independent neurite branching in human neuroblastoma cells. J. Cell Sci. *116*, 1925–1935.
48. Anastasaki, C., Estep, A.L., Marais, R., Rauen, K.A., and Patton, E.E. (2009). Kinase-activating and kinase-impaired cardio-facio-cutaneous syndrome alleles have activity during zebrafish development and are sensitive to small molecule inhibitors. Hum. Mol. Genet. *18*, 2543–2554.

nature genetics

Variants in *CPA1* are strongly associated with early onset chronic pancreatitis

Heiko Witt[1–3], Sebastian Beer[4,44], Jonas Rosendahl[5,44], Jian-Min Chen[6,7,44], Giriraj Ratan Chandak[8,44], Atsushi Masamune[9,44], Melinda Bence[4,44], Richárd Szmola[4,10,44], Grzegorz Oracz[11], Milan Macek Jr[12], Eesh Bhatia[13], Sandra Steigenberger[1,2], Denise Lasher[1,2], Florence Bühler[1,2], Catherine Delaporte[1,2], Johanna Tebbing[1,2], Maren Ludwig[1,2], Claudia Pilsak[1,2], Karolin Saum[1,2], Peter Bugert[14], Emmanuelle Masson[6,7], Sumit Paliwal[8], Seema Bhaskar[8], Agnieszka Sobczynska-Tomaszewska[15,16], Daniel Bak[16], Ivan Balascak[17], Gourdas Choudhuri[18], D Nageshwar Reddy[19], G Venkat Rao[19], Varghese Thomas[20], Kiyoshi Kume[9], Eriko Nakano[9], Yoichi Kakuta[9], Tooru Shimosegawa[9], Lukasz Durko[21], András Szabó[4], Andrea Schnúr[4,22], Péter Hegyi[22], Zoltán Rakonczay Jr[22], Roland Pfützer[23], Alexander Schneider[24], David Alexander Groneberg[25], Markus Braun[25], Hartmut Schmidt[26], Ulrike Witt[27], Helmut Friess[27], Hana Algül[28], Olfert Landt[29], Markus Schuelke[30,31], Renate Krüger[32], Bertram Wiedenmann[33], Frank Schmidt[34], Klaus-Peter Zimmer[35], Peter Kovacs[36,37], Michael Stumvoll[36,37], Matthias Blüher[36,37], Thomas Müller[38], Andreas Janecke[38,39], Niels Teich[40], Robert Grützmann[41], Hans-Ulrich Schulz[42], Joachim Mössner[5], Volker Keim[5], Matthias Löhr[43], Claude Férec[6,7] & Miklós Sahin-Tóth[4]

Chronic pancreatitis is an inflammatory disorder of the pancreas. We analyzed *CPA1*, encoding carboxypeptidase A1, in subjects with nonalcoholic chronic pancreatitis (cases) and controls in a German discovery set and three replication sets. Functionally impaired variants were present in 29/944 (3.1%) German cases and 5/3,938 (0.1%) controls (odds ratio (OR) = 24.9, $P = 1.5 \times 10^{-16}$). The association was strongest in subjects aged ≤10 years (9.7%; OR = 84.0, $P = 4.1 \times 10^{-24}$). In the replication sets, defective *CPA1* variants were present in 8/600 (1.3%) cases and 9/2,432 (0.4%) controls from Europe ($P = 0.01$), 5/230 (2.2%) cases and 0/264 controls from India ($P = 0.02$) and 5/247 (2.0%) cases and 0/341 controls from Japan ($P = 0.013$). The mechanism by which *CPA1* variants confer increased pancreatitis risk may involve misfolding-induced endoplasmic reticulum stress rather than elevated trypsin activity, as is seen with other genetic risk factors for this disease.

Chronic pancreatitis is an inflammatory condition that is characterized by abdominal pain and progressive damage to both exocrine and endocrine components of the pancreas, resulting in insufficiency of the organ with maldigestion and diabetes. Although alcohol abuse has long been recognized as a major risk factor for chronic pancreatitis, genetic susceptibility has emerged during the last two decades as a strong determinant of disease risk, particularly in the pediatric population[1].

Genetic studies performed so far have suggested that the development of intrapancreatic trypsin activity has a central role in disease pathogenesis. Thus, gain-of-function mutations in the gene encoding cationic trypsinogen (*PRSS1*, MIM276000) as well as loss-of-function variants in the genes encoding the pancreatic secretory trypsin inhibitor (*SPINK1*, MIM167790) and the trypsinogen-degrading enzyme chymotrypsin C (*CTRC*, MIM601405) increase the risk for chronic pancreatitis[2–8]. Consistent with the proposed pathogenic role of trypsin, a rapidly autodegrading variant of the gene encoding anionic trypsinogen (*PRSS2*, MIM601564) and a common *PRSS1* promoter variant protect against chronic pancreatitis[9,10].

Despite these recent advances, we still find that many individuals with chronic pancreatitis do not carry mutations in any of the known susceptibility genes, suggesting the involvement of other yet unidentified genes. In the present study, we investigated the role of *CPA1* in individuals with chronic pancreatitis. Digestive carboxypeptidases are pancreatic metalloproteases that hydrolyze C-terminal peptide bonds in dietary polypeptide chains[11]. Three different isoforms have been described in human pancreatic juice. A-type carboxypeptidases (CPA1 and CPA2) act on aromatic and aliphatic amino acid residues that are exposed by the action of chymotrypsins and elastases, whereas the B-type carboxypeptidase (CPB1) hydrolyzes C-terminal lysine and arginine residues generated by tryptic cleavages[11]. The gene encoding human CPA1 (MIM114850) maps to 7q32.2, spans approximately 8 kb and contains 10 exons. The inactive preproprotein comprises 419 amino acids, including a

A full list of author affiliations appears at the end of the paper.

Received 18 April; accepted 23 July; published online 18 August 2013; doi:10.1038/ng.2730

Table 1 Nonsynonymous *CPA1* variants in German subjects with nonalcoholic chronic pancreatitis and healthy controls

Exon	Nucleotide change	Amino acid change	Cases (%) (n = 944)	Controls (%) (n = 3,938)	P	OR	95% CI	Apparent activity	Secretion level
1	c.5G>A	p.Arg2Gln	0 (0)	2 (0.05)	1.0	–	–	103	92
2	**c.79C>T**	**p.Arg27Ter**	**0 (0)**	**2 (0.05)**	**1.0**	**–**	**–**	**0**	**0**
2	c.101C>T	p.Ala34Val	0 (0)	1 (0.03)	1.0	–	–	98	97
3	c.197G>A	p.Arg66Gln	0 (0)	2 (0.05)	1.0	–	–	60	55
3	c.281A>G	p.Gln94Arg	1 (0.1)	13 (0.3)	0.5	–	–	57	57
3	c.321C>G	p.Phe107Leu	0 (0)	1 (0.03)	1.0	–	–	112	100
3	c.371C>T	p.Thr124Ile	8 (0.9)	45 (1.1)	0.6	–	–	23	27
4	c.410C>G	p.Ala137Gly	1 (0.1)	0 (0)	0.2	–	–	52	56
5	c.497G>A	p.Gly166Asp	5 (0.5)	20 (0.5)	1.0	–	–	73	66
5	**c.542G>A**	**p.Arg181Gln**	**0 (0)**	**1 (0.03)**	**1.0**	**–**	**–**	**1**	**39**
6	c.622G>A	p.Ala208Thr (het)	71 (7.5)	266 (6.8)	0.4	–	–	81	73
6	c.622G>A	p.Ala208Thr (hom)	1 (0.1)	1 (0.03)	0.4	–	–	–	–
6	c.622G>T	p.Ala208Ser	0 (0)	1 (0.03)	1.0	–	–	91	83
6	**c.673G>A**	**p.Gly225Ser**	**1 (0.1)**	**0 (0)**	**0.2**	**–**	**–**	**4**	**12**
7	**c.710G>A**	**p.Arg237His**	**0 (0)**	**2 (0.05)**	**1.0**	**–**	**–**	**0**	**81**
7	**c.751G>A**	**p.Val251Met**	**2 (0.2)**	**0 (0)**	**0.1**	**–**	**–**	**0**	**0**
7	**c.758C>G**	**p.Pro253Arg**	**1 (0.1)**	**0 (0)**	**0.2**	**–**	**–**	**0**	**0**
7	**c.768C>G**	**p.Asn256Lys**	**7 (0.7)**	**0 (0)**	**9.9×10^{-6}**	**NC**	**NC**	**0**	**0**
7	c.775G>A	p.Ala259Thr	0 (0)	1 (0.03)	1.0	–	–	85	82
8	**c.811T>C**	**p.Cys271Arg**	**1 (0.1)**	**0 (0)**	**0.2**	**–**	**–**	**1**	**0**
8	**c.829G>A**	**p.Gly277Ser**	**1 (0.1)**	**0 (0)**	**0.2**	**–**	**–**	**0**	**0**
8	**c.839C>A**	**p.Ala280Asp**	**1 (0.1)**	**0 (0)**	**0.2**	**–**	**–**	**0**	**5**
8	**c.847G>A**	**p.Glu283Lys**	**2 (0.2)**	**0 (0)**	**0.1**	**–**	**–**	**0**	**0**
8	**c.982G>A**	**p.Glu328Lys**	**1 (0.1)**	**0 (0)**	**0.2**	**–**	**–**	**9**	**42**
9	c.1009G>C	p.Val337Leu	0 (0)	1 (0.03)	1.0	–	–	64	61
Intron 9	**c.1073-2A>G**	**p.Tyr358fs[a]**	**3 (0.3)**	**0 (0)**	**0.007**	**NC**	**NC**	**0**	**0**
10	**c.1085G>A**	**p.Gly362Glu**	**1 (0.1)**	**0 (0)**	**0.2**	**–**	**–**	**0**	**6**
10	**c.1126T>C**	**p.Ser376Pro**	**2 (0.2)**	**0 (0)**	**0.1**	**–**	**–**	**0**	**7**
10	**c.1144C>T**	**p.Arg382Trp**	**5 (0.5)**	**0 (0)**	**0.0003**	**NC**	**NC**	**0**	**31**
10	c.1157G>A	p.Arg386His	0 (0)	1 (0.03)	1.0	–	–	92	97
10	c.1193C>T	p.Pro398Leu	0 (0)	1 (0.03)	1.0	–	–	42	64
10	c.1217C>G	p.Ala406Gly	0 (0)	1 (0.03)	1.0	–	–	137	114
10	**c.1247delA**	**p.Asn416fs**	**1 (0.1)**	**0 (0)**	**0.2**	**–**	**–**	**11**	**15**
10	c.1251C>A	p.His417Gln	0 (0)	1 (0.03)	1.0	–	–	62	54
10	c.1253C>T	p.Pro418Leu	0 (0)	1 (0.03)	1.0	–	–	91	99
All variants with apparent activity <20%			**29 (3.1%)**	**5 (0.1)**	**1.5×10^{-16}**	**24.9**	**9.6–64.6**	–	–

P values were determined by Fisher's exact test. Apparent CPA1 activity and secretion levels are expressed as a percentage of the wild-type values. Apparent activity corresponds to the CPA1 activity measured in the conditioned medium of transfected cells after activation with trypsin and CTRC (Online Methods). Thus, the apparent activity reflects the combined effects of the variants on secretion, catalytic activity and degradation by trypsin and/or CTRC. Secretion level indicates the concentration of proCPA1 in the conditioned medium measured by SDS-PAGE and densitometry (Online Methods). Alterations in bold indicate variants with less than 20% apparent activity.

[a]A splice-site variant that was modeled functionally as intron retention (as described in the **Supplementary Note**). Het, heterozygous; hom, homozygous; NC, not calculated, as the variant was not detected in the controls, rendering the OR infinite.

16-amino-acid secretory signal peptide and a 94-amino-acid propeptide. Activation of the proenzyme (proCPA1) to CPA1 is catalyzed by the sequential action of trypsin and CTRC, which cleave and degrade the propeptide[12]. After trypsinogens, proCPA1 is the second largest component of pancreatic juice, contributing more than 10% of the total protein[13].

We performed direct DNA sequencing of all ten *CPA1* exons in 944 cases and 3,938 control subjects of German origin. Considering variants in the coding regions and flanking splice sites, we identified 31 missense variants, 1 nonsense variant, 1 frame-shift variant and 1 splice-site variant and found that 3 variants were significantly enriched in cases (**Table 1**). Functional analysis demonstrated that 17/34 (50%) variants resulted in a marked (>80%) loss of apparent CPA1 activity, a term we use to describe the combined effects of the variants on secretion, proteolytic stability and catalytic competence (**Table 1**, **Supplementary Fig. 1** and Online Methods). The majority of these variants were located in exons 7, 8 and 10. Notably, 14 out of 17 (82%) functionally impaired variants were present in cases exclusively, including the c.768C>G (p.Asn256Lys) variant, which we detected in seven cases. Thus, *CPA1* variants with less than 20% apparent activity were significantly over-represented in the chronic pancreatitis group (29/944, 3.1%) as compared to in controls (5/3,938, 0.1%) (OR = 24.9, 95% confidence interval (CI) 9.6–64.6, $P = 1.5 \times 10^{-16}$) (**Table 1**). No individual was compound heterozygous or

Table 2 Distribution of functionally impaired *CPA1* variants in different age groups of German subjects with nonalcoholic chronic pancreatitis

Age of cases	Cases (%)	Controls (%)	P	OR	95% CI
All	29/944 (3.1)	5/3,938 (0.1)	1.5×10^{-16}	24.9	9.6–64.6
>20 years	2/358 (0.6)	5/3,938 (0.1)	0.2	–	–
≤20 years	27/586 (4.6)	5/3,938 (0.1)	6.8×10^{-20}	38.0	14.6–99.1
≤10 years	22/228 (9.7)	5/3,938 (0.1)	4.1×10^{-24}	84.0	31.5–224.1

P values were determined by Fisher's exact test. Alterations with less than 20% apparent activity were included.

Table 3 Nonsynonymous *CPA1* variants in the European replication study

Exon	Nucleotide change	Amino acid change	Cases (%) (n = 600)	Controls (%) (n = 2,432)	P	OR	95% CI	Apparent activity	Secretion level
1	c.5G>A	p.Arg2Gln	0 (0)	6 (0.2)	0.6	–	–	103	92
2	**c.79C>T**	**p.Arg27Ter**	**1 (0.2)**	**5 (0.2)**	**0.7**	**–**	**–**	**0**	**0**
2	**c.80G>C**	**p.Arg27Pro**	**0 (0)**	**1 (0.04)**	**1.0**	**–**	**–**	**0**	**0**
Intron 2	**c.148-1G>A**	**p.Leu50_Glu127del[a]**	**0 (0)**	**1 (0.04)**	**1.0**	**–**	**–**	**0**	**0**
3	c.197G>A	p.Arg66Gln	0 (0)	1 (0.04)	1.0	–	–	60	55
3	c.241T>C	p.Ser81Pro	0 (0)	1 (0.04)	1.0	–	–	53	57
3	c.281A>G	p.Gln94Arg	0 (0)	9 (0.4)	1.0	–	–	57	57
3	c.313T>C	p.Phe105Leu	1 (0.2)	0 (0)	0.2	–	–	109	99
3	c.334C>T	p.Arg112Cys	1 (0.2)	0 (0)	0.2	–	–	69	78
3	c.371C>T	p.Thr124Ile	3 (0.5)	14 (0.6)	1.0	–	–	23	27
4	c.389A>C	p.Asp130Ala	0 (0)	1 (0.04)	1.0	–	–	77	68
5	c.497G>A	p.Gly166Asp	1 (0.2)	11 (0.5)	0.5	–	–	73	66
6	c.604C>A	p.Gln202Lys	1 (0.2)	0 (0)	0.2	–	–	114	104
6	c.622G>A	p.Ala208Thr	45 (7.5)[b]	143 (5.9)[b]	0.1	–	–	81	73
6	**c.686C>T**	**p.Thr229Met**	**0 (0)**	**1 (0.04)**	**1.0**	**–**	**–**	**0**	**0**
6	c.695C>T	p.Thr232Met	1 (0.2)	0 (0)	0.2	–	–	87	80
7	**c.751G>A**	**p.Val251Met**	**1 (0.2)**	**0 (0)**	**0.2**	**–**	**–**	**0**	**0**
8	**c.809C>G**	**p.Pro270Arg**	**1 (0.2)**	**0 (0)**	**0.2**	**–**	**–**	**9**	**14**
8	**c.941A>G**	**p.Tyr314Cys**	**1 (0.2)**	**0 (0)**	**0.2**	**–**	**–**	**0**	**23**
8	**c.954_955delCA**	**p.Tyr318Ter**	**2 (0.3)**	**0 (0)**	**0.04**	**NC**	**NC**	**0**	**0**
9	c.1010T>C	p.Val337Ala	0 (0)	1 (0.04)	1.0	–	–	63	90
Intron 9	**c.1072+1G>T**	**p.Asp330fs[a]**	**0 (0)**	**1 (0.04)**	**1.0**	**–**	**–**	**0**	**0**
Intron 9	**c.1073-2A>G**	**p.Tyr358fs[a]**	**1 (0.2)**	**0 (0)**	**0.2**	**–**	**–**	**0**	**0**
10	c.1115G>A	p.Gly372Asp	1[c] (0.2)	0 (0)	0.2	–	–	25	34
10	c.1203G>C	p.Lys401Asn	1 (0.2)	0 (0)	0.2	–	–	115	103
10	**c.1217C>T**	**p.Ala406Val**	**1 (0.2)**	**0 (0)**	**0.2**	**–**	**–**	**0**	**87**
All variants with apparent activity <20%			**8 (1.3)**	**9 (0.4)**	**0.01**	**3.6**	**1.4–9.5**	**–**	**–**

P values were determined by Fisher's exact test. Apparent CPA1 activity and secretion levels were measured as described in **Table 1** and are expressed as a percentage of the wild-type values. Alterations in bold indicate variants with less than 20% apparent activity.
[a]The functional effects of the splice-site variants c.148-1G>A, c.1072+1G>T and c.1073-2A>G were modeled as skipping of exon 3, skipping of exon 9 and retention of intron 9, respectively (as described in the **Supplementary Note**). [b]One individual was homozygous for p.Ala208Thr. [c]This individual was homozygous for this variant. NC, not calculated, as the variant was not detected in controls, rendering the OR infinite.

homozygous for a defective *CPA1* variant. Variants located in noncoding regions and synonymous variants located in coding regions are listed in **Supplementary Table 1**.

We observed that cases bearing a defective *CPA1* variant were younger than those without a *CPA1* alteration. In the German chronic pancreatitis group, the majority of *CPA1* variants with less than 20% apparent activity were present in cases at or below 20 years of age (27/586, 4.6%) (OR = 38.0, 95% CI 14.6–99.1, $P = 6.8 \times 10^{-20}$). This finding was even more significant in a subgroup of cases at or below 10 years of age. In this group, 22/228 (9.7%) carried an impaired *CPA1* variant (OR = 84.0, 95% CI 31.5–224.1, $P = 4.1 \times 10^{-24}$) (cases ≤10 years of age compared to cases ≤20 years of age, $P = 0.007$; cases ≤10 years of age compared to all cases, $P = 7.6 \times 10^{-5}$) (**Table 2**).

We also investigated all *CPA1* exons in 465 German subjects with alcohol-related chronic pancreatitis. Only 2/465 (0.4%) of these individuals were heterozygous for a defective *CPA1* variant: c.954_955delCA (p.Tyr318Ter) in one individual and c.811T>C (p.Cys271Arg) in the other. This indicates that loss-of-function alterations in *CPA1* have a minor role in alcoholic pancreatitis.

To confirm the association of nonalcoholic chronic pancreatitis and *CPA1* in an independent European cohort, we sequenced all *CPA1* exons in 600 cases and 2,432 control subjects originating from France, the Czech Republic and Poland. Again, variants with less than 20% apparent activity were significantly over-represented in chronic pancreatitis cases (8/600, 1.3%) compared to in ethnically matched controls (9/2,432, 0.4%) (OR = 3.6, 95% CI 1.4–9.5, $P = 0.01$) (**Table 3**). One subject with chronic pancreatitis was homozygous for the c.1115G>A (p.Gly372Asp) variant.

To investigate the significance of *CPA1* variants in subjects of non-European descent, we sequenced all ten exons in 230 cases and 264 controls of Indian origin and 247 cases and 341 controls from Japan. Overall, 2.2% (5/230) of the Indian cases but none of the controls

Table 4 Nonsynonymous *CPA1* variants in Indian subjects with nonalcoholic chronic pancreatitis and healthy controls

Exon	Nucleotide change	Amino acid change	Cases (%) (n = 230)	Controls (%) (n = 264)	P	OR	95% CI	Apparent activity	Secretion level
2	c.94G>C	p.Asp32His	1 (0.4)	0 (0)	0.5	–	–	79	75
5	c.506G>A	p.Arg169His	4 (1.7)	0 (0)	0.046	NC	NC	24	23
6	c.622G>A	p.Ala208Thr	6 (2.6)	7 (2.7)	1.0	–	–	81	73
8	**c.922T>C**	**p.Tyr308His**	**5 (2.2)**	**0 (0)**	**0.02**	**NC**	**NC**	**3**	**17**
All variants with apparent activity <20%			**5 (2.2)**	**0 (0)**	**0.02**	**NC**	**NC**	**–**	**–**

P values were determined by Fisher's exact test. Apparent CPA1 activity and secretion levels were measured as described in **Table 1** and are expressed as a percentage of the wild-type values. Alterations in bold indicate variants with less than 20% apparent activity. NC, not calculated, as the variant was not detected in controls, rendering the OR infinite.

Table 5 Nonsynonymous *CPA1* variants in Japanese subjects with nonalcoholic chronic pancreatitis and healthy controls

Exon	Nucleotide change	Amino acid change	Cases (%) (n = 247)	Controls (%) (n = 341)	P	OR	95% CI	Apparent activity	Secretion level
4	c.410C>G	p.Ala137Gly	1 (0.4)	0 (0)	0.42	–	–	52	56
7	**c.713A>T**	**p.Lys238Met**	**1 (0.4)**	**0 (0)**	**0.42**	–	–	**0**	**3**
7	**c.751G>A**	**p.Val251Met**	**2 (0.8)**	**0 (0)**	**0.18**	–	–	**0**	**0**
7	**c.764G>T**	**p.Arg255Met**	**1 (0.4)**	**0 (0)**	**0.42**	–	–	**0**	**86**
9	c.1021G>A	p.Ala341Thr	37 (15.0)	53 (15.5)	1.0	–	–	99	85
10	**c.1079-27_1111dup60**	**p.Thr368_Tyr369ins20[a]**	**1 (0.4)**	**0 (0)**	**0.42**	–	–	**0**	**49**
All variants with apparent activity <20%			**5 (2.0)**	**0 (0)**	**0.013**	**NC**	**NC**	–	–

P values were determined by Fisher's exact test. Apparent CPA1 activity and secretion levels were measured as described in **Table 1** and are expressed as a percentage of the wild-type values. Alterations in bold indicate variants with less than 20% apparent activity.
[a]The functional effect of the variant c.1079-27_1111dup60 was modeled as an insertion of 20 amino acids between Thr368 and Tyr369 (as described in the **Supplementary Note**).
NC, not calculated, as the variant was not detected in controls, rendering the OR infinite.

carried a defective *CPA1* variant ($P = 0.02$) (**Table 4**). In the Japanese sample collection, 2.0% (5/247) of the cases but none of the controls carried an impaired *CPA1* variant ($P = 0.013$) (**Table 5**). No individual from India or Japan was compound heterozygous or homozygous for a defective *CPA1* variant.

Chronic pancreatitis is a complex multigenic disease, and affected individuals often carry mutations in several disease-associated genes. To elucidate the relationship between *CPA1* alterations and *PRSS1*, *SPINK1*, *CTRC* and *CFTR* variants, we investigated all German subjects with chronic pancreatitis for variants in *PRSS1* (encoding p.Ala16Val, p.Asn29Ile and p.Arg122His), *SPINK1* (encoding p.Asn34Ser and c.194+2T>C), *CTRC* (encoding p.Arg254Trp and p.Lys247_Arg254del) and *CFTR* (encoding p.Phe508del). In total, 50/944 (5.3%) individuals carried a heterozygous *PRSS1* variant, 147/944 (15.6%) were positive for *SPINK1* p.Asn34Ser (121 heterozygotes and 18 homozygotes) and c.194+2T>C (20 heterozygotes, 12 of which were compound heterozygous with p.Asn34Ser), 28/944 (3.0%) were positive for a *CTRC* variant (21 instances of p.Arg254Trp and 7 occurrences of p.Lys247_Arg254del), and 42/944 (4.5%) were positive for *CFTR* p.Phe508del. Together, 273/944 (28.9%) of the cases showed at least one of the above-mentioned genetic alterations, and 24/944 (2.5%) of the cases were *trans* heterozygous. However, only 1/29 (3.6%) cases with a defective *CPA1* variant was *trans* heterozygous; this subject carried the *CPA1* c.1073-2A>G alteration (inherited from the mother) and the *SPINK1* p.Asn34Ser variant (inherited from the father). This suggests a limited interaction of *CPA1* variants with variants in other susceptibility genes and stands in contrast with the high number of *trans* heterozygotes for *SPINK1*, *CTRC* and/or *CFTR* variants, as was described recently[14].

The mechanism by which loss-of-function *CPA1* variants predispose to chronic pancreatitis is not intuitively apparent. We found no detectable effect of CPA1 on trypsinogen activation, trypsin activity or degradation of trypsin and trypsinogen by CTRC (**Supplementary Fig. 2**), indicating that *CPA1* variants do not exert their effect by increasing intrapancreatic trypsin activity. However, the low apparent activity of most of the defective variants was due to markedly reduced secretion (**Tables 1–5** and **Supplementary Figs. 1** and **3**), raising the possibility that CPA1 mutants misfold in the endoplasmic reticulum and cause endoplasmic reticulum stress, as has been demonstrated previously for some PRSS1 and CTRC mutants[15,16]. Indeed, expression of the most frequently found p.Asn256Lys variant in AR42J rat acinar cells resulted in endoplasmic reticulum stress, as evidenced by increased splicing of *Xbp1* and elevated mRNA levels of the chaperones *Hspa5* (encoding BiP) and *Calr* (encoding calreticulin) (**Fig. 1**). Considering that CPA1 is one of the most abundant proteins synthesized by the pancreas, misfolding-induced endoplasmic reticulum stress seems to be a plausible mechanism to explain the clinical effects of heterozygous CPA1 variants.

In summary, loss-of-function *CPA1* variants are strongly associated with nonalcoholic chronic pancreatitis, especially early onset disease. Although there was evidence of heterogeneity in the spectrum of variants present in different populations, the identification of functionally impaired *CPA1* variants in both European and non-European sample collections establishes its global role in the pathogenesis of chronic pancreatitis.

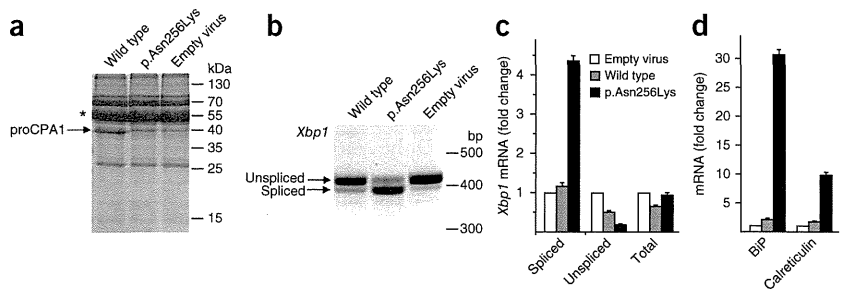

Figure 1 Endoplasmic reticulum stress induced by the p.Asn256Lys CPA1 variant. (**a**) AR42J rat acinar cells were transfected with the indicated wild-type, mutant or empty adenovirus vectors for 24 h using 4×10^7 plaque-forming units (pfu) per ml of virus. Conditioned media (200 µl) were precipitated with trichloroacetic acid (10% final concentration) and analyzed by SDS-PAGE and Coomassie blue staining. The p.Asn256Lys mutant had a complete lack of secretion. The faint band at 40 kDa represents an endogenous protein also found in the medium from cells infected with the empty virus. The asterisk indicates the characteristically strong amylase band. See the Online Methods for experimental details. A representative gel of three independent transfections is shown. (**b**) *Xbp1* splicing was assessed by RT-PCR and agarose gel electrophoresis with ethidium bromide staining. A representative gel of three independent experiments is shown. (**c**) Levels of spliced, unspliced and total *Xbp1* mRNA were measured by quantitative real-time PCR and are expressed as fold changes relative to the levels measured in cells transfected with empty adenovirus. (**d**) Quantitative real-time PCR measurements of *Hspa5* (encoding BiP) and *Calr* (encoding calreticulin) mRNA were performed as described in the Online Methods and are expressed as fold changes relative to the levels measured in cells transfected with empty adenovirus. Error bars (**c**,**d**), s.d. (n = 3 independent experiments).

METHODS

Methods and any associated references are available in the online version of the paper.

Accession codes. GenBank: carboxypeptidase A1 (*CPA1*), NT_007933.15 (*Homo sapiens* chromosome 7 genomic contig, GRCh37.p5); NM_001868.2 (human *CPA1* mRNA sequence).

Note: Any Supplementary Information and Source Data files are available in the online version of the paper.

ACKNOWLEDGMENTS

The authors thank all study participants and the members of the Gesellschaft für Pädiatrische Gastroenterologie und Ernährung (GPGE) for providing clinical data and blood samples. The authors also thank C. Ruffert (Leipzig), K. Krohn, K. Schön and B. Oelzner (Interdisziplinäres Zentrum für Klinische Forschung (IZKF) core unit DNA technologies, Leipzig), V. Sahin-Tóth (Boston) and K.R. Mani (CCMB, Hyderabad) for excellent technical assistance. This work was supported by the Deutsche Forschungsgemeinschaft (DFG) grants Wi 2036/2-2 and Wi 2036/2-3 (to H.W.) and RO 3929/1-1 and RO 3939/2-1 (to J.R.), the Else Kröner-Fresenius-Foundation (EKFS) (to H.W.), a grant of the Colora Stiftung gGmbH (to J.R.), US National Institutes of Health (NIH) grants R01DK058088, R01DK082412, R01DK082412-S2 and R01DK095753 (to M.S.-T.), fellowships from the Roszstoczy Foundation (to M. Bence and A. Schnúr), the Bolyai postdoctoral fellowship from the Hungarian Academy of Sciences (to R.S.), INSERM, the Programme Hospitalier de Recherche Clinique (PHRC R 08-04), the French Association des Pancréatites Chroniques Héréditaires and its president N. Meslet, the Czech Ministry of Health conceptual development project of research organization University Hospital Motol in Prague (00064203) and grants CZ.2.16/3.1.00/24022OPPK (to M.M.), the Council of Scientific and Industrial Research (CSIR), Ministry of Science and Technology, Government of India, India grant GENESIS (to G.R.C.), a Grant-in-Aid from the Japan Society for the Promotion of Science (#23591008 to A.M.) and the Research Committee of Intractable Pancreatic Diseases provided by the Ministry of Health, Labour and Welfare of Japan (to A.M. and T.S.).

AUTHOR CONTRIBUTIONS

H.W. and M.S.-T. conceived, designed and directed the study. G.R.C., J.-M.C., J.R., A.M. and H.W. designed, performed and interpreted genetic analyses with substantial contributions from D.B., F.B., M. Braun, S. Bhaskar, C.D., D.L., E.M., S.P., S.S., A.S.-T., K.K., E.N., Y.K., T.S., J.T. and A. Schneider. S. Beer, M. Bence, R.S., A. Szabó, A. Schnúr and M.S.-T. carried out functional characterization of CPA1 variants. H.W., M.S.-T. and S. Beer wrote the manuscript with substantial contributions from G.R.C., J.-M.C., J.R. and A.M. O.L. provided oligonucleotides. All other coauthors recruited study subjects, collected clinical data and provided genomic DNA samples. All authors approved the final manuscript and contributed critical revisions to its intellectual content.

COMPETING FINANCIAL INTERESTS

The authors declare no competing financial interests.

1. Witt, H., Apte, M.V., Keim, V. & Wilson, J.S. Chronic pancreatitis: challenges and advances in pathogenesis, genetics, diagnosis, and therapy. *Gastroenterology* **132**, 1557–1573 (2007).
2. Whitcomb, D.C. *et al.* Hereditary pancreatitis is caused by a mutation in the cationic trypsinogen gene. *Nat. Genet.* **14**, 141–145 (1996).
3. Witt, H., Luck, W. & Becker, M. A signal peptide cleavage site mutation in the cationic trypsinogen gene is strongly associated with chronic pancreatitis. *Gastroenterology* **117**, 7–10 (1999).
4. Le Maréchal, C. *et al.* Hereditary pancreatitis caused by triplication of the trypsinogen locus. *Nat. Genet.* **38**, 1372–1374 (2006).
5. Witt, H. *et al.* Mutations in the gene encoding the serine protease inhibitor, Kazal type 1 are associated with chronic pancreatitis. *Nat. Genet.* **25**, 213–216 (2000).
6. Chandak, G.R. *et al.* Mutations in the pancreatic secretory trypsin inhibitor gene (*PSTI/SPINK1*) rather than the cationic trypsinogen gene (*PRSS1*) are significantly associated with tropical calcific pancreatitis. *J. Med. Genet.* **39**, 347–351 (2002).
7. Rosendahl, J. *et al.* Chymotrypsin C (*CTRC*) variants that diminish activity or secretion are associated with chronic pancreatitis. *Nat. Genet.* **40**, 78–82 (2008).
8. Masson, E., Chen, J.M., Scotet, V., Le Maréchal, C. & Férec, C. Association of rare chymotrypsinogen C (*CTRC*) gene variations in patients with idiopathic chronic pancreatitis. *Hum. Genet.* **123**, 83–91 (2008).
9. Witt, H. *et al.* A degradation-sensitive anionic trypsinogen (*PRSS2*) variant protects against chronic pancreatitis. *Nat. Genet.* **38**, 668–673 (2006).
10. Whitcomb, D.C. *et al.* Common genetic variants in the *CLDN2* and *PRSS1-PRSS2* loci alter risk for alcohol-related and sporadic pancreatitis. *Nat. Genet.* **44**, 1349–1354 (2012).
11. Vendrell, J., Querol, E. & Avilés, F.X. Metallocarboxypeptidases and their protein inhibitors. Structure, function and biomedical properties. *Biochim. Biophys. Acta* **1477**, 284–298 (2000).
12. Szmola, R. *et al.* Chymotrypsin C is a co-activator of human pancreatic procarboxypeptidases A1 and A2. *J. Biol. Chem.* **286**, 1819–1827 (2011).
13. Scheele, G., Bartelt, D. & Bieger, W. Characterization of human exocrine pancreatic proteins by two-dimensional isoelectric focusing/sodium dodecyl sulfate gel electrophoresis. *Gastroenterology* **80**, 461–473 (1981).
14. Rosendahl, J. *et al. CFTR, SPINK1, CTRC* and *PRSS1* variants in chronic pancreatitis: is the role of mutated *CFTR* overestimated? *Gut* **62**, 582–592 (2013).
15. Kereszturi, E. *et al.* Hereditary pancreatitis caused by mutation-induced misfolding of human cationic trypsinogen: a novel disease mechanism. *Hum. Mutat.* **30**, 575–582 (2009).
16. Beer, S. *et al.* Comprehensive functional analysis of chymotrypsin C (*CTRC*) variants reveals distinct loss-of-function mechanisms associated with pancreatitis risk. *Gut* doi:10.1136/gutjnl-2012-303090 (1 September 2012).

[1]Else Kröner-Fresenius-Zentrum für Ernährungsmedizin (EKFZ), Technische Universität München (TUM), Freising, Germany. [2]Zentralinstitut für Ernährungs- und Lebensmittelforschung (ZIEL), TUM, Freising, Germany. [3]Department of Pediatrics, Klinikum Rechts der Isar (MRI), TUM, Munich, Germany. [4]Department of Molecular and Cell Biology, Boston University Henry M. Goldman School of Dental Medicine, Boston, Massachusetts, USA. [5]Department for Internal Medicine, Neurology and Dermatology, Division of Gastroenterology, University of Leipzig, Leipzig, Germany. [6]Institut National de la Santé et de la Recherche Médicale (INSERM), U1078, Etablissement Français du Sang (EFS)–Bretagne, Brest, France. [7]Faculté de Médecine et des Sciences de la Santé, Université de Bretagne Occidentale, Brest, France. [8]Centre for Cellular and Molecular Biology (CCMB), Council of Scientific and Industrial Research (CSIR), Hyderabad, India. [9]Division of Gastroenterology, Tohoku University Graduate School of Medicine, Sendai, Miyagi, Japan. [10]2nd Department of Medicine, Semmelweis University, Budapest, Hungary. [11]Department of Gastroenterology, Hepatology and Immunology, The Children's Memorial Health Institute, Warsaw, Poland. [12]Department of Biology and Medical Genetics, University Hospital Motol and 2nd Faculty of Medicine of Charles University Prague, Prague, Czech Republic. [13]Department of Endocrinology, Sanjay Gandhi Postgraduate Institute of Medical Sciences, Lucknow, India. [14]Institute of Transfusion Medicine and Immunology, Medical Faculty Mannheim, Heidelberg University, Mannheim, Germany. [15]MedGen Health Care Centre, Warsaw, Poland. [16]Department of Medical Genetics, Institute of Mother and Child, Warsaw, Poland. [17]Clinic of Obstetrics and Gynecology, Department of Neonatology, University Hospital Motol and 2nd Medical School, Charles University Prague, Prague, Czech Republic. [18]Department of Gastroenterology, Sanjay Gandhi Postgraduate Institute of Medical Sciences, Lucknow, India. [19]Asian Institute of Gastroenterology, Hyderabad, India. [20]Department of Gastroenterology, Medical College Hospital, Calicut, India. [21]Department of Digestive Tract Diseases, Medical University of Lodz, Lodz, Poland. [22]1st Department of Medicine, University of Szeged, Szeged, Hungary. [23]Department of Internal Medicine, Klinikum Döbeln, Döbeln, Germany. [24]Department of Medicine II, Universitätsmedizin Mannheim, Ruprecht-Karls-Universität Heidelberg, Mannheim, Germany. [25]Institute for Occupational Medicine, Goethe-Universität Frankfurt, Frankfurt, Germany. [26]Department for Transplant Medicine, University Hospital Münster, Albert-Schweitzer-Campus 1, Münster, Germany. [27]Department of Surgery, TUM, Munich, Germany. [28]Department of Gastroenterology, TUM, Munich, Germany. [29]TIB MOLBIOL, Berlin, Germany. [30]Department of Neuropediatrics, Charité, Campus Virchow-Klinikum, Berlin, Germany. [31]NeuroCure Clinical Research Center, Charité, Campus Virchow-Klinikum, Berlin, Germany. [32]Department of Pediatrics, Division of Pediatric Pulmonology, Charité, Campus Virchow-Klinikum, Berlin, Germany. [33]Department of Internal Medicine, Division of Hepatology and Gastroenterology, Charité, Campus Virchow-Klinikum, Berlin, Germany. [34]Department of Pediatrics, University of Halle-Wittenberg, Halle (Saale), Germany. [35]Department of Pediatrics, Justus-Liebig-Universität, Gießen, Germany. [36]Department for Internal Medicine, Neurology and Dermatology, Division of Endocrinology, University of Leipzig, Leipzig, Germany. [37]Integriertes Forschungs- und Behandlungszentrum (IFB) Adiposity Diseases, University of Leipzig, Leipzig, Germany. [38]Universitätsklinik für Pädiatrie I, Department für Kinder-und Jugendheilkunde, Medizinische Universität Innsbruck, Innsbruck, Austria. [39]Sektion für Humangenetik, Medizinische Universität Innsbruck, Innsbruck, Austria. [40]Practice for Digestive and Metabolic Diseases, Leipzig, Germany. [41]Department of Surgery, Universitätsklinikum Dresden, Dresden, Germany. [42]Department of Surgery, Otto-von-Guericke University Magdeburg, Magdeburg, Germany. [43]Department of Clinical Science, Intervention and Technology, Karolinska Institutet, Karolinska University Hospital Huddinge, Stockholm, Sweden. [44]These authors contributed equally to this work. Correspondence should be addressed to H.W. (heiko.witt@lrz.tum.de) or M.S.-T. (miklos@bu.edu).

ONLINE METHODS

Study population. The medical ethical review committees of all participating study centers approved this study. All study subjects gave informed consent. We enrolled 944 unrelated German individuals with a diagnosis of nonalcoholic chronic pancreatitis and 465 subjects with alcohol-related chronic pancreatitis. In the replication study, we investigated 600 unrelated subjects with nonalcoholic chronic pancreatitis originating from France (n = 456), the Czech Republic (n = 21) and Poland (n = 123). In addition, we investigated unrelated subjects affected with nonalcoholic chronic pancreatitis from India (n = 230) and Japan (n = 247). The diagnosis of chronic pancreatitis was based on two or more of the following findings: presence of a typical history of recurrent pancreatitis, pancreatic calcifications and/or pancreatic ductal irregularities revealed by endoscopic retrograde pancreaticography or by magnetic resonance imaging of the pancreas, and/or pathological sonographic findings. Alcoholic chronic pancreatitis was diagnosed in subjects who consumed more than 60 g (females) or 80 g (males) of ethanol per day for more than 2 years. Control subjects were recruited from Germany (n = 3,938), France (n = 2,000), the Czech Republic (n = 235), Poland (n = 197), India (n = 264) and Japan (n = 341).

Mutation screening. We designed primers complementary to intronic sequences flanking *CPA1* exons on the basis of the published nucleotide sequence (GenBank NT_007933.15) (**Supplementary Table 2**). After PCR amplification, the entire coding region and the exon-intron boundaries were sequenced. All mutations were confirmed with a second independent PCR reaction. In the German laboratories, we performed PCR using 0.75 U AmpliTaq Gold polymerase (Perkin Elmer), 400 μmol/l deoxynucleoside triphosphates and 0.1 μmol/l primers in a total volume of 25 μl. The cycle conditions were as follows: initial denaturation for 12 min at 95 °C; 48 cycles of 20 s denaturation at 95 °C, 40 s annealing at 64 °C and 90 s primer extension at 72 °C; and a final extension step for 2 min at 72 °C. PCR products were digested with Antarctic phosphatase (New England Biolabs) or shrimp alkaline phosphatase (USB) and exonuclease I (New England Biolabs). Cycle sequencing was performed using BigDye terminator mix (Applied Biosystems) with a 56 °C annealing temperature. The reaction products were purified with ethanol precipitation and loaded onto an ABI 3730 or ABI 3100-Avant fluorescence sequencer (Applied Biosystems).

Functional characterization of CPA1 variants. We investigated the functional consequences of *CPA1* alterations by transient transfection of HEK 293T cells (#Q401, GenHunter) with wild-type and mutant constructs and analyzing the conditioned medium for the amount of proCPA1 protein constitutively secreted using densitometry of stained gels and CPA1 activity after activation with trypsin and CTRC.

Expression plasmids, mutagenesis and adenoviruses. Construction of the pcDNA3.1(-) human *CPA1* expression plasmid has been reported previously[12]. The coding DNA in this plasmid was derived from IMAGE clone #3949850 (GenBank accession BC005279), which contains a c.827A>G (p.His276Arg) alteration. This error was corrected by back mutating Arg276 to histidine. *CPA1* mutants were created by PCR mutagenesis and ligated into the pcDNA3.1(-) expression plasmid. Recombinant adenoviruses carrying wild-type *CPA1* or the p.Asn256Lys mutant were generated by Viraquest. Details regarding the construction of the *CPA1* splice-site and duplication mutant expression plasmids are provided in the **Supplementary Note**.

Cell culture and transfection. HEK 293T cells were cultured in six-well tissue culture plates (1.5×10^6 cells per well) in DMEM (Invitrogen) supplemented with 10% fetal bovine serum, 4 mM glutamine and 1% penicillin and streptomycin at 37 °C. Transfections were carried out at 90% confluence using 10 μl Lipofectamine 2000 (Invitrogen) and 4 μg expression plasmids in a final volume of 2 ml DMEM. After overnight incubation, cells were washed, and the transfection medium was replaced with 2 ml OPTI-MEM I Reduced Serum Medium (Invitrogen). The conditioned OPTI-MEM media were harvested after 48 h of incubation. AR42J rat pancreatic acinar cells (American Type Culture Collection #CRL-1492) were maintained in DMEM supplemented with 20% fetal bovine serum, 4 mM glutamine and 1% penicillin and streptomycin at 37 °C. Before transfection, cells were plated in six-well plates (10^6 cells per well) and grown in the presence of a 100 nM concentration of dexamethasone for 48 h to induce differentiation. Infections with adenoviruses were performed using 4×10^7 pfu per ml of the final adenovirus concentrations in a total volume of 1 ml OPTI-MEM in the presence of dexamethasone (100 nM final concentration).

CPA1 activity assay. The enzymatic activity of CPA1 was determined after activation with trypsin and CTRC using the N-[4-methoxyphenylazoformyl]-L-phenylalanine substrate[17] with minor modifications of our previously published conditions[12]. The CPA1 activity measured in the conditioned medium of transfected cells is referred to as the 'apparent activity' and reflects the combined effects of the variants on the secreted amounts of proCPA1, the proteolytic degradation during activation and the catalytic activity of the activated CPA1. To activate proCPA1, an aliquot (20 μl) of the conditioned medium was supplemented with 0.1 M Tris-HCl (pH 8.0), 1 mM $CaCl_2$, 0.05% Tween 20, 100 nM human cationic trypsin and 50 nM human CTRC (final concentrations in a final volume of 40 μl) and incubated at 37 °C for 60 min. CPA1 activity was then measured by adding 50 μl assay buffer (0.1 M Tris-HCl (pH 8.0), 1 mM $CaCl_2$ and 0.05% Tween 20) and 10 μl substrate (final concentration of 60 μM) to the activation mix. The decrease in absorbance was followed at 350 nm for 2 min. Rates of substrate cleavage were calculated from fits to the initial linear portion of the curves and are expressed as a percentage of the wild-type rate, which was set to 100%. The wild-type activity corresponded to 116 ± 34 milliOD min^{-1} (average ± s.d.), which equals a 262 ± 77 nM s^{-1} substrate cleavage rate.

Measurement of proCPA1 secretion. Secreted amounts of proCPA1 protein in the conditioned medium were determined by SDS-PAGE and densitometry. An aliquot (200 μl) of the medium was precipitated with trichloroacetic acid (10% final concentration), the precipitate was recovered by centrifugation, dissolved in 20 μl Laemmli sample buffer containing 100 mM dithiothreitol (DTT) (final concentration) and heat denatured at 95 °C for 5 min. Electrophoretic separation was performed on 15% SDS-PAGE mini gels in standard Tris-glycine buffer, and gels were stained with Brilliant Blue R-250. Quantification of bands was carried out with the GelDocXR+ gel documentation system and Image Lab 3.0 software (Bio-Rad).

Measurement of endoplasmic reticulum stress. To study endoplasmic reticulum stress, we generated recombinant adenoviruses carrying either wild-type *proCPA1* or the p.Asn256Lys mutant, infected AR42J rat pancreatic acinar cells (#CRL-1492, American Type Culture Collection (ATCC)) with these viruses and measured endoplasmic reticulum stress markers as described below.

RT-PCR analysis and real-time PCR. Total RNA was extracted from AR42J cell lysates using an RNeasy mini kit (Qiagen). RNA was reverse transcribed using the High Capacity cDNA Reverse Transcription Kit (Applied Biosystems). *Xbp1* (encoding X-box binding protein 1) splicing was studied by PCR using a primer set that flanked the spliced region and amplified both the spliced and unspliced forms (**Supplementary Table 3**). PCR was carried out using the *Taq* DNA Polymerase kit (Qiagen) with the following conditions: 10 min initial denaturation at 95 °C followed by 35 cycles of 30 s denaturation at 95 °C, 30 s annealing at 52 °C, 30 s extension at 72 °C and a final extension at 72 °C for 5 min. The PCR products were resolved on 2% agarose gels and stained with ethidium bromide. Quantification of mRNA expression was performed by real-time PCR (7500 Real Time PCR System, Applied Biosystems). *Xbp1* expression was measured with SYBR Green (PCR Master Mix, Applied Biosystems) using different primer sets for the spliced, unspliced and total mRNA (**Supplementary Table 3**). Levels of *Hspa5* (encoding the immunoglobulin-binding protein BiP) and *Calr* (encoding calreticulin) mRNA were determined using TaqMan primers (rat *Hspa5*, Rn00565250_m1; rat *Calr*, Rn00574451_m1) with TaqMan Universal PCR Mastermix (Applied Biosystems). Real-time PCR conditions were as follows: 2 min equilibration at 50 °C, 10 min denaturation and enzyme activation at 95 °C followed by 40 two-step cycles of 15 s at 95 °C and 60 s at 60 °C. Gene expression was quantified using the comparative C_T method ($\Delta\Delta C_T$ method). Threshold cycle (C_T) values were determined using the 7500 System Sequence Detection Software 1.3.

Expression levels of target genes were first normalized to the *Gapdh* internal control gene (ΔC_T) and then to the expression levels measured in cells infected with empty adenovirus ($\Delta\Delta C_T$). Results were expressed as fold changes calculated with the formula $2^{-\Delta\Delta CT}$.

Statistics. The significance of the differences between mutation frequencies in affected individuals and controls was tested by two-tailed Fisher's exact test. Additional ORs were calculated using SAS/STAT software (v 9.1) and GraphPad Prism (v 4.03).

17. Mock, W.L., Liu, Y. & Stanford, D.J. Arazoformyl peptide surrogates as spectrophotometric kinetic assay substrates for carboxypeptidase A. *Anal. Biochem.* **239**, 218–222 (1996).

CLINICAL REPORT

AMERICAN JOURNAL OF medical genetics PART A

A Transient Myelodysplastic/Myeloproliferative Neoplasm in a Patient With Cardio-Facio-Cutaneous Syndrome and a Germline *BRAF* Mutation

Kazuhito Sekiguchi,[1]* Tomoki Maeda,[1] So-ichi Suenobu,[1,2] Nobutaka Kunisaki,[1] Miki Shimizu,[1] Kyoko Kiyota,[1] Yo-suke Handa,[1] Kensuke Akiyoshi,[1] Seigo Korematsu,[1,3] Yoko Aoki,[4] Yoichi Matsubara,[4] and Tatsuro Izumi[1]

[1]Department of Pediatrics and Child Neurology, Oita University Faculty of Medicine, Oita, Japan

[2]Division of General Pediatrics and Emergency Medicine, Oita University Faculty of Medicine, Oita, Japan

[3]Educational Support for Regional Pediatrics, Oita University Faculty of Medicine, Oita, Japan

[4]Department of Medical Genetics, Tohoku University School of Medicine, Sendai, Japan

Manuscript Received: 4 March 2013; Manuscript Accepted: 26 May 2013

A male infant, born at 32 weeks gestation by cesarean because of hydrops fetalis, presented with multiple anomalies, such as sparse and curly scalp hair, absent eyebrows, frontal bossing, an atrial septal defect, pulmonary artery stenosis, and whole myocardial thickening. He was clinically diagnosed with cardio-facio-cutaneous (CFC) syndrome, and was confirmed to have a germline V-raf murine sarcoma viral oncogene homologue B1 (*BRAF*) c.721 A>C mutation. At 1 month of age, he presented with a transient myelodysplastic/myeloproliferative neoplasm (MDS/MPN), which improved within a month without the administration of antineoplastic agents. This is the first report of CFC syndrome with MDS/MPN. The coexistence of MDS/MPN may be related to this *BRAF* c.721 A>C mutation. © 2013 Wiley Periodicals, Inc.

Key words: cardio-facio-cutaneous syndrome; myelodysplastic/myeloproliferative neoplasm; BRAF; RAS/MAPK syndromes; juvenile myelomonocytic leukemia

How to Cite this Article:
Sekiguchi K, Maeda T, Suenobu S-I, Kunisaki N, Shimizu M, Kiyota K, Handa Y-S, Akiyoshi K, Korematsu S, Aoki Y, Matsubara Y, Izumi T. 2013. A transient myelodysplastic/myeloproliferative neoplasm in a patient with cardio-facio-cutaneous syndrome and a germline BRAF mutation.
Am J Med Genet Part A 161A:2600–2603.

INTRODUCTION

Cardio-facio-cutaneous (CFC) syndrome is genetic disorder characterized by clinical features such as congenital heart defects, a characteristic facial appearance, ectodermal abnormalities and growth failure [Reynolds et al., 1986]. V-raf murine sarcoma viral oncogene homolog B1 (*BRAF*) is one of rat sarcoma viral oncogene homolog/mitogen activated protein kinase (RAS/MAPK) signaling pathway genes, and has been identified as a causative gene of CFC syndrome [reviewed in Aoki et al., 2008 and Denayer and Legius, 2007]. We report on a male infant with CFC syndrome, who was confirmed to have a germline *BRAF* mutation, and then presented with a myelodysplastic/myeloproliferative neoplasm (MDS/MPN) at 1 month of age.

CLINICAL REPORT

A male was born through cesarean at 32 weeks gestation as the first product of healthy nonconsanguineous Japanese parents. His birth weight, length and head circumference were 2,370 g (−0.8 SD), 40.0 cm (+2.3 SD), 34.2 cm (+3.2 SD), respectively. Due to hydrops fetalis and neonatal asphyxia, he required immediate resuscitation. Mechanical ventilation was needed until age 3 months. He presented with multiple anomalies, such as sparse and curly scalp hair, absent eyebrows, frontal bossing with temporal narrowing, ocular hypertelorism, low set ears, a short and webbed neck, and cryptorchidism (Fig. 1). His complete blood counts at age 1 day revealed the following: WBC 12,770/μl (neutrophils 80%,

Conflict of interest: none.

*Correspondence to:
Kazuhito Sekiguchi, Department of Pediatrics and Child Neurology, Oita University Faculty of Medicine, 1-1 Idaigaoka, Hasama, Yufu, Oita 879-5593, Japan.
E-mail: sekiguch@oita-u.ac.jp

Article first published online in Wiley Online Library (wileyonlinelibrary.com): 15 August 2013
DOI 10.1002/ajmg.a.36107

FIG. 1. Full-body image of the patient at birth and his facial features at 3 hours of age. The patient showed severe generalized edema at birth. He presented with sparse and curly hair, frontal bossing, hypertelorism, low-set ears, a short and webbed neck, and cryptorchidism.

lymphocytes 12%, monocytes 6%, myelocytes 2%), RBC 343 × 10^4/μl, erythroblasts 2,430/μl, hemoglobin 14.2g/dl, and platelets 3.2 × 10^4/μl. A chromosome analysis of his peripheral blood lymphocytes showed a 46, XY karyotype. He had an atrial septal defect (ASD), pulmonary artery stenosis (PS), whole myocardial thickening, a pulmonary arteriovenous fistula, an intrahepatic portal systemic shunt, hepatosplenomegaly, right cryptorchidism, a right double renal pelvis, and ureter and agenesis of the corpus callosum. These clinical features were all compatible with CFC syndrome.

At age 1 month, a peripheral blood examination indicated monocytosis of 17% (2,370/μl), with WBC 13,930/μl, RBC 295 × 10^4/μl, and platelets 11.2 × 10^4/μl, with giant platelets. Bone marrow aspiration revealed a nucleated cell count of 9.4 × 10^4/μl, megakaryocyte count 56.2/μl, and did not contain pathologic blasts. The karyotype of the bone marrow cells was 46, XY. The granulocyte-macrophage colony-forming unit (CFU-GM) assay using a semi-solid methylcellulose method showed spontaneous CFU-GM formation of bone marrow (5/5 × 10^4 mononuclear cells) and peripheral blood (35/5 × 10^4 mononuclear cell), without growth factors. Based on these laboratory findings, this patient was diagnosed with MDS/MPN. However, the peripheral blood monocytosis improved without the administration of antineoplastic agents after 1 month with 13% monocytes (1,140/μl), WBC of 8,780/μl, RBC 314 × 10^4/μl, and platelets 26.3 × 10^4/μl. At age 3 years, his complete blood counts revealed 11% monocytes (903/μl), WBC 8,210/μl, RBC 428 × 10^4/μl, and platelets 31.1 × 10^4/μl (Table I). He smiled normally. He demonstrated generalized hypotonia without normal head control and was unable to produce meaningful speech.

CYTOGENETIC AND GENOMIC ANALYSIS

The *BRAF* sequencing analysis showed a heterozygous A>C change at nucleotide 721, resulting in a p.T241P amino acid change in exon 6, which was a previously known mutation in CFC syndrome [Schulz et al., 2008]. No mutations were noted in the Kirsten rat sarcoma viral oncogene homologue (*KRAS*) or protein-tyrosine phosphatase, nonreceptor-type11 (*PTPN11*).

DISCUSSION

A male infant, born via cesarean section because of hydrops fetalis, presented with multiple anomalies suggestive of CFC syndrome. A pulmonary arteriovenous fistula, an intrahepatic portal systemic shunt, hepatosplenomegaly, cryptorchidism, a double renal pelvis, and ureter have been reported as rare complications in CFC syndrome [Narumi et al., 2007]. At 1 month of age, he presented with MDS/MPN, which improved within a month. He showed a germline mutation of *BRAF* c.721 A>C, resulting in a p.T241P amino acid change in exon 6, within a cysteine-rich domain. This mutation was previously described in CFC syndrome [Schulz et al., 2008].

The clinical findings of CFC syndrome are similar to those of other RAS/MAPK or neuro-cardio-facial-cutaneous syndromes, such as Noonan and Costello syndrome [reviewed in Aoki et al., 2008; Denayer and Legius, 2007]. The RAS/MAPK signaling pathway genes, not only *BRAF*, but also *KRAS*, MAPK kinase/ERK kinase 1 (*MEK1*), and MAPK kinase/ERK kinase2 (*MEK2*) have been reported as causative genes for CFC syndrome [Niihori et al., 2006; Rodriguez-Viciana et al., 2006]. CFC syndrome had been considered to have a low risk of malignancy among the various RAS/MAPK syndromes, but a few patients with CFC syndrome due to *BRAF* mutation have presented with malignancies, such as acute lymphoblastic leukemia [van Den Berg and Hennekam, 1999; Makita et al., 2007], and precursor T-lymphoblastic lymphoma [Ohtake et al., 2011].

MDS/MPNs include clonal myeloid neoplasms that at the time of initial presentation have clinical, laboratory or morphologic findings supporting a diagnosis of MDS, and other findings more consistent with MPN. They are usually characterized by hypercellularity of the

TABLE I. Peripheral Blood Examinations of This Patient

Age (months)	0	1	2	12	21	38
WBC (/μl)	12,770	13,930	8,730	8,660	9,040	8,210
Monocytes (/μl)	766	2,370	1,140	866	633	903
RBC (×10^4/μl)	343	295	314	396	404	428
Platelets (×10^4/μl)	3.2	11.2	26.3	24.2	38.6	31.1

bone marrow due to proliferation in one or more of the myeloid lineages [Swerdlow et al., 2008]. Juvenile myelomonocytic leukemia (JMML) is one type of MDS/MPN. Peripheral blood and bone marrow from JMML patients demonstrate spontaneous proliferation according to a CFU-GM assay [Estrov et al., 1986]. Transient monocytosis is not rare in preterm infants [Rajadurai et al., 1992]. Monocytosis in preterm infants is not usually considered a sign of MPD/MPN. In this case, the monocytes proliferation independent of growth factors was noticed according to a CFU-GM assay. The spontaneous proliferation was in favor of MPN. In RAS/MAPK syndromes, occasionally young infants with Noonan syndrome develop a JMML-like disorder which spontaneously resolves without treatment in some, and behaves more aggressively in others [Bader-Meunier et al., 1997; reviewed in Choong et al., 1999]. These children carried germline mutations in *PTPN11* [Tartaglia et al., 2003] or in *KRAS* [Kratz et al., 2005]. *BRAF* mutations had not previously been detected in patients with JMML [de Vries et al., 2007]. This is the first report of a germline *BRAF* mutation and MDS/MPN in a patient with CFC syndrome. The MDS/MPN improved without the administration of antineoplastic agents. This clinical course is similar to the JMML-like disorder observed in Noonan syndrome. This suggests a common mechanism for the development and progression of MDS/MPN in patients with RAS/MAPK syndromes. The MDS/MPN in RAS/MAPK syndrome patients has parallels with the transient leukemia of newborns with Down syndrome. However, the transient leukemia associated with Down syndrome has a high concentration of blasts in the peripheral blood and a GATA binding protein 1 (*GATA1*) mutation as somatic molecular marker [Xu et al., 2003].

The germline *BRAF* mutation site of this patient, c.721 A>C in exon 6, had been reported in two previous patients. One had CFC syndrome [Schulz et al., 2008], and the other had Noonan syndrome with multiple lentigines, previously referred to as LEOPARD syndrome [Sarkozy et al., 2009]. These two patients did not present with malignancies. Garnett and Marais [2004] reviewed the *BRAF* mutations in various adult cancers, and showed that up to 90% of mutations occurred in exon 12. The *BRAF* mutation site of this patient, exon 6, may be related to the spontaneous improvement of his MDS/MPN. A long-term follow-up and additional bone marrow assays might be needed if the patient demonstrates suspicious symptoms with or without peripheral blood monocytosis, because of the risk that MDS/MPN may recur. Further accumulated data about CFC syndrome with a *BRAF* mutation may help to elucidate the basic mechanisms of malignancy, and may suggest a therapeutic strategy.

ACKNOWLEDGMENTS

The authors are grateful to Drs. Hideki Muramatsu and Seiji Kojima, Department of Pediatrics/Developmental Pediatrics, Nagoya University Graduate School of Medicine, Nagoya, for providing important data from the colony assay.

REFERENCES

Aoki Y, Niihori T, Narumi Y, Kure S, Matsubara Y. 2008. The RAS/MAPK syndromes: novel roles of the RAS pathway in human genetic disorders. Hum Mutat 29:992–1006. Review.

Bader-Meunier B, Tchernia G, Miélot F, Fontaine JL, Thomas C, Lyonnet S, Lavergne JM, Dommergues JP. 1997. Occurrence of myelodysplastic/myeloproliferative neoplasm in patients with Noonan syndrome. J Pediatr 130:885–889.

Choong K, Freedman MH, Chitayat D, Kelly EN, Taylor G, Zipursky A. 1999. Juvenile myelomonocytic leukemia and Noonan syndrome. J Pediatr Hematol Oncol 21:523–527. Review.

de Vries AC, Stam RW, Kratz CP, Zenker M, Niemeyer CM, van den Heuvel-Eibrink MM. European Working Group on childhood MDS (EWOG-MDS). 2007. Mutation analysis of the *BRAF* oncogene in juvenile myelomonocytic leukemia. Haematologica 92:1574–1575.

Denayer E, Legius E. 2007. What's new in the neuro-cardio-facial-cutaneous syndromes? Eur J Pediatr 166:1091–1098. Review.

Estrov Z, Grunberger T, Chan HS, Freedman MH. 1986. Juvenile chronic myelogenous leukemia: characterization of the disease using cell cultures. Blood 67:1382–1387.

Garnett MJ, Marais R. 2004. Guilty as charged: *B-RAF* is a human oncogene. Cancer Cell 6:313–319. Review.

Kratz CP, Niemeyer CM, Castleberry RP, Cetin M, Bergsträsser E, Emanuel PD, Hasle H, Kardos G, Klein C, Kojima S, Stary J, Trebo M, Zecca M, Gelb BD, Tartaglia M, Loh ML. 2005. The mutational spectrum of *PTPN11* in juvenile myelomonocytic leukemia and Noonan syndrome/myeloproliferative disease. Blood 106:2183–2185.

Makita Y, Narumi Y, Yoshida M, Niihori T, Kure S, Fujieda K, Matsubara Y, Aoki Y. 2007. Leukemia in Cardio-facio-cutaneous (CFC) syndrome: a patient with a germline mutation in *BRAF* proto-oncogene. J Pediatr Hematol Oncol 29:287–290.

Narumi Y, Aoki Y, Niihori T, Neri G, Cavé H, Verloes A, Nava C, Kavamura MI, Okamoto N, Kurosawa K, Hennekam RC, Wilson LC, Gillessen-Kaesbach G, Wieczorek D, Lapunzina P, Ohashi H, Makita Y, Kondo I, Tsuchiya S, Ito E, Sameshima K, Kato K, Kure S, Matsubara Y. 2007. Molecular and clinical characterization of cardio-facio-cutaneous (CFC) syndrome: Overlapping clinical manifestations with Costello syndrome. Am J Med Genet Part A 143A:799–807.

Niihori T, Aoki Y, Narumi Y, Neri G, Cavé H, Verloes A, Okamoto N, Hennekam RC, Gillessen-Kaesbach G, Wieczorek D, Kavamura MI, Kurosawa K, Ohashi H, Wilson L, Heron D, Bonneau D, Corona G, Kaname T, Naritomi K, Baumann C, Matsumoto N, Kato K, Kure S, Matsubara Y. 2006. Germline *KRAS* and *BRAF* mutations in cardio-facio-cutaneous syndrome. Nat Genet 38:294–296.

Ohtake A, Aoki Y, Saito Y, Niihori T, Shibuya A, Kure S, Matsubara Y. 2011. Non-Hodgkin lymphoma in a patient with cardiofaciocutaneous syndrome. J Pediatr Hematol Oncol 33:e342–e346.

Rajadurai VS, Chambers HM, Vigneswaran R, Gardiner AA. 1992. Monocytosis in preterm infants. Early Hum Dev. 28:223–229.

Reynolds JF, Neri G, Herrmann JP, Blumberg B, Coldwell JG, Miles PV, Opitz JM. 1986. New multiple congenital anomalies/mental retardation syndrome with cardio-facio-cutaneous involvement—The CFC syndrome. Am J Med Genet 25:413–427.

Rodriguez-Viciana P, Tetsu O, Tidyman WE, Estep AL, Conger BA, Cruz MS, McCormick F, Rauen KA. 2006. Germline mutations in genes within the MAPK pathway cause cardio-facio-cutaneous syndrome. Science 311:1287–1290.

Sarkozy A, Carta C, Moretti S, Zampino G, Digilio MC, Pantaleoni F, Scioletti AP, Esposito G, Cordeddu V, Lepri F, Petrangeli V, Dentici ML, Mancini GM, Selicorni A, Rossi C, Mazzanti L, Marino B, Ferrero GB, Silengo MC, Memo L, Stanzial F, Faravelli F, Stuppia L, Puxeddu E, Gelb BD, Dallapiccola B, Tartaglia M. 2009. Germline *BRAF* mutations in Noonan, LEOPARD, and cardiofaciocutaneous syndromes: Molecular diversity and associated phenotypic spectrum. Hum Mutat 30:695–702.

Schulz AL, Albrecht B, Arici C, van der Burgt I, Buske A, Gillessen-Kaesbach G, Heller R, Horn D, Hübner CA, Korenke GC, König R, Kress W, Krüger G, Meinecke P, Mücke J, Plecko B, Rossier E, Schinzel A, Schulze A, Seemanova E, Seidel H, Spranger S, Tuysuz B, Uhrig S, Wieczorek D, Kutsche K, Zenker M. 2008. Mutation and phenotypic spectrum in patients with cardio-facio-cutaneous and Costello syndrome. Clin Genet 73:62–70.

Swerdlow SH, Campo E, Harris NL, Jaffe ES, Pileri SA, Stein H, Thiele J, Vardiman JW. 2008. World Health Organization classification of tumours of haematopoietic and lymphoid tissues. Lyon: International Agency for Research on Cancer.

Tartaglia M, Niemeyer CM, Fragale A, Song X, Buechner J, Jung A, Hählen K, Hasle H, Licht JD, Gelb BD. 2003. Somatic mutations in *PTPN11* in juvenile myelomonocytic leukemia, myelodysplastic syndromes and acute myeloid leukemia. Nat Genet 34:148–150.

van Den Berg H, Hennekam RC. 1999. Acute lymphoblastic leukaemia in a patient with cardiofaciocutaneous syndrome. J Med Genet 36:799–800.

Xu G, Nagano M, Kanezaki R, Toki T, Hayashi Y, Taketani T, Taki T, Mitui T, Koike K, Kato K, Imaizumi M, Sekine I, Ikeda Y, Hanada R, Sako M, Kudo K, Kojima S, Ohneda O, Yamamoto M, Ito E. 2003. Frequent mutations in the *GATA-1* gene in the transient myeloproliferative disorder of Down syndrome. Blood 102:2960–2968.

OPEN ACCESS

RESEARCH PAPER

Clinical features and a mutation with late onset of limb girdle muscular dystrophy 2B

Toshiaki Takahashi,[1] Masashi Aoki,[2] Naoki Suzuki,[2] Maki Tateyama,[2] Chikako Yaginuma,[3] Hitomi Sato,[3] Miho Hayasaka,[3,4] Hitomi Sugawara,[3] Mariko Ito,[3,5] Emi Abe-Kondo,[3,6] Naoko Shimakura,[2] Tohru Ibi,[7,8] Satoshi Kuru,[9] Tadashi Wakayama,[9,10] Gen Sobue,[11] Naoki Fujii,[12] Toshio Saito,[13] Tsuyoshi Matsumura,[13] Itaru Funakawa,[14] Eiichiro Mukai,[15] Toru Kawanami,[16] Mitsuya Morita,[17] Mineo Yamazaki,[18] Takashi Hasegawa,[19,20] Jun Shimizu,[21] Shoji Tsuji,[21] Shigeki Kuzuhara,[22,23] Hiroyasu Tanaka,[1] Masaru Yoshioka,[1,3] Hidehiko Konno,[1] Hiroshi Onodera,[1] Yasuto Itoyama[2,24]

► Additional supplementary files are published online only. To view these files please visit the journal online (http://dx.doi.org/10.1136/jnnp-2011-301339).

For numbered affiliations see end of article

Correspondence to
Dr M Aoki, Department of Neurology, Tohoku University School of Medicine, 1-1 Seiryo-machi, Sendai 980-8574, Japan; aokim@med.tohoku.ac.jp

Received 2 September 2011
Revised 18 April 2012
Accepted 13 May 2012
Published Online First 15 December 2012

ABSTRACT

Objective and methods Dysferlin encoded by *DYSF* deficiency leads to two main phenotypes, limb girdle muscular dystrophy (LGMD) 2B and Miyoshi myopathy. To reveal in detail the mutational and clinical features of LGMD2B in Japan, we observed 40 Japanese patients in 36 families with LGMD2B in whom dysferlin mutations were confirmed.

Results and conclusions Three mutations (c.1566C>G, c.2997G>T and c.4497delT) were relatively more prevalent. The c.2997G>T mutation was associated with late onset, proximal dominant forms of dysferlinopathy, a high probability that muscle weakness started in an upper limb and lower serum creatine kinase (CK) levels. The clinical features of LGMD2B are as follows: (1) onset in the late teens or early adulthood, except patients homozygous for the c.2997G>T mutation; (2) lower limb weakness at onset; (3) distal change of lower limbs on muscle CT at an early stage; (4) impairment of lumbar erector spinal muscles on muscle CT at an early stage; (5) predominant involvement of proximal upper limbs; (6) preservation of function of the hands at late stage; (7) preservation of strength in neck muscles at late stage; (8) lack of facial weakness or dysphagia; (9) avoidance of scoliosis; (10) hyper-Ckaemia; (11) preservation of cardiac function; and (12) a tendency for respiratory function to decline with disease duration. It is important that the late onset phenotype is found with prevalent mutations.

INTRODUCTION

Dysferlinopathies are autosomal recessive muscular dystrophies caused by mutations in the dysferlin gene (*DYSF*, MIM# 603009). Dysferlin deficiency leads to two main phenotypes: limb girdle muscular dystrophy (LGMD) 2B and Miyoshi myopathy (MM).[1 2] Dysferlin is located on the plasma membrane of skeletal muscle and is deficient in patients with MM and LGMD2B.[3 4] However, atypical immunostaining in muscle from patients with dysferlin mutations occurs,[5 6] and dysferlin expression is not normal in sarcoglycanopathy, dystrophinopathy,[7] caveolinopathy[8 9] or calpainopathy[6] muscles. Therefore, the final diagnosis of dysferlinopathy requires identification of mutations in the dysferlin gene. We first reported dysferlin mutations in Japanese patients with MM[10] and in a patient from a non-European ethnic group with distal anterior compartment myopathy (DACM),[11] a relatively new phenotype of dysferlinopathy.[12] Furthermore, we revealed that, in MM, four mutations (c.1566C>G, c.2997G>T, c.3373delG and c.4497delT) were relatively more prevalent in the Japanese population and the c.2997G>T mutation was associated with late onset.[13] Although mutation analysis of the dysferlin gene is a time consuming task because of the large size of the gene,[14] large series of patients with dysferlin gene mutations have been studied.[6 15–24] However, few detailed analyses of the clinical features of LGMD2B, especially in relation to various types of mutations, have been reported. Here we report the clinical features of a series of 40 patients in 36 families with LGMD2B in whom dysferlin mutations were confirmed, and cardiac and respiratory functions were involved. In particular, we took into account the duration that had elapsed since onset when the clinical data were examined.

MATERIALS AND METHODS

We retrospectively observed 40 Japanese patients in 36 families with LGMD2B in whom dysferlin mutations were confirmed. LGMD was defined as symptomatic myopathy excluding MM and DACM at the first visit to a neurologist. Mutational analysis was performed by single strand conformation polymorphism analysis and sequencing on genomic DNA using our previously reported method,[13 14 25] with minor modifications (Ref Seq NM_003494.2), and with informed consent and approval of our local ethics committee. We retrospectively reassessed the history of onset and progression of the disease. The clinical examination included manual muscle testing using the Medical Research Council (MRC) Scale and assignment of scales for the proximal limb muscles, as proposed by Brooke *et al*.[26] Clinical examination was carried out by neurologists from the study groups for muscular dystrophy in Japan.

Most patients had undergone muscle CT scans at some stage of the disease. Serum creatine kinase (CK) activity was measured. Cardiac and respiratory functions were evaluated. We selected the first and last manual muscle testing data and the last data on the scales for the proximal limb muscles, CK activity, cardiac function and respiratory function. We used all muscle CT scans. Patients were divided into three groups according to whether they had the homozygous c.2997G>T (p.Trp999Cys) mutation, the heterozygous c.2997G>T (p.Trp999Cys) mutation or other mutations. Difference in age at onset among the groups was evaluated by the Kruskal–Wallis test. Multiple comparison of age at onset between each group was assessed by Scheffé's F test. Difference in the first symptom among the groups was evaluated by the χ^2 for independence test. Kaplan–Meier curves with log rank test were used to examine survival at each milestone of progression in the groups. Pearson's correlation coefficient test was used to identify significant associations in ejection fraction (EF) (n=21), atrial natriuretic peptide (n=9), brain natriuretic peptide (n=7), per cent vital capacity (%VC) (n=23), carbon dioxide partial pressure (pCO_2) (n=16) and oxygen partial pressure (pO_2) (n=16) with disease duration. Because supine and standing position chest x-rays were mingled, Pearson's correlation coefficient test was not used for the cardiothoracic ratio (n=22).

RESULTS

Mutations

We identified 17 different mutations in 36 families (table 1). Two mutations (c.2974T>C (p.Trp992Arg) and c.2997G>T (p.Trp999Cys)) were missense mutations and four mutations (c.342+1G>A, c.937+1G>A, c.2643+1G>A and c.4794 +1G>A) were splice site mutations. The others were nonsense mutations. The c.2997G>T (p.Trp999Cys) mutation was present in 26 alleles (36.1%). The c.1566C>G (p.Tyr522X) mutation and the c.4497delT mutation were both present in eight alleles (11.1%). We identified the c.3373delG mutation that has high frequency in Japanese patients with MM[13] in only one allele.

Clinical course

Mean age at onset of all patients was 26.6±9.9 years (range 14–58): the group homozygous for the c.2997G>T (p.Trp999Cys) mutation, 37.9±10.2 years (19–58); the group heterozygous for the c.2997G>T (p.Trp999Cys) mutation, 26.8 ±7.6 years (14–35); and the group without the c.2997G>T (p.Trp999Cys) mutation, 21.8±5.8 years (14–41). The difference between the group homozygous for the c.2997G>T (p.Trp999Cys) mutation and the group heterozygous for the c.2997G>T (p.Trp999Cys) mutation was significant ($p<0.05$). The difference between the group homozygous for the c.2997G>T (p.Trp999Cys) mutation and the group without the c.2997G>T (p.Trp999Cys) mutation was significant ($p<0.01$) (figure 1). The first symptom in most patients was lower limb weakness. Walking on tiptoe was the first sign in one patient. In three patients with the homozygous c.2997G>T (p.Trp999Cys) mutation, the first symptom was upper limb weakness. In two patients, one of them carrying the homozygous c.2997G>T (p.Trp999Cys) mutation, upper limb weakness was concomitant with lower limb weakness. There was a significant difference ($p<0.01$) in the probability that the first symptom was upper limb weakness among these three groups. The first symptom in one patient was left brachial pain and in another patient it was limitation of the elbow, hip, knee and spine.[27] In the early stage of the clinical course, hypertrophy of the calves was noticed in three patients. Winged scapula, rigid spine[27] and hollow foot were observed in one patient each. Lordosis was observed in two patients. Weakness of the face, dysphagia, scoliosis and kyphosis were not found. Choreic movements and pollakisuria were found in one patient.[28] Mean duration at difficulty in running was 1.3 years from disease onset (range 0–10), 3.1 years (0–14) for difficulty in climbing stairs, 5.5 years (0–16) for stumbling, 6.0 years (0–10) for difficulty in standing on tiptoe, 6.7 years (0–15) for rising from the floor, 8.7 years (0–25) for noticing weakness in a proximal upper limb, 12.5 years (3–23) for walking with a cane, 20.4 years (9–35) for noticing weakness in a distal upper limb, 21.6 years (13–29) for using a wheelchair and 31.0 years (16–45) for using an electric wheelchair. There was a significant difference ($p<0.05$) in the survival ratio only at the stage of difficulty in standing on tiptoe among these three groups (figure 2). There were no significant differences in survival at the stage of the other symptoms between these three groups. According to the scales for the proximal limb muscles, only two patients each reached the severest stage of arms and shoulders (cannot raise hands to mouth and have no useful function) and hips and legs (confined to bed).

Manual muscle testing

In the first decade of the disease, the muscles of the lower limbs were predominantly involved. In the upper limbs, the deltoid muscle was predominantly involved. In the second decade of the disease, the biceps and triceps brachii muscles became weak. Later on, the flexor and extensor of the hand became weak. Muscle weakness progressed and, in the fifth decade of the disease, the muscles of the lower limbs were very weak (1 on the MRC Scale). In the patient with 52 years of disease duration, although the muscles of the upper and the lower limbs were 0 on the MRC scale, the flexor and extensor of the neck were relatively preserved (2 on the MRC Scale).

Muscle CT scans

The CT scans revealed low density changes in the gastrocnemius, especially in the medial heads, soleus, hamstrings and the erector spinal group, which was mainly affected in the lateral parts in the early disease stage. Low density abnormalities in the quadriceps femoris and the adductor magnus muscles were observed at close to 10 years after disease onset. The tibialis anterior, the peroneal group, the gluteal group, the quadrates lumborum and the deltoid muscles were involved at 10 years after onset. The gracilis and sarcorius muscles were preserved and had hypertrophied during the second decade of disease duration. Approximately 20 years after disease onset, low density changes in the dorsal muscles occurred in the neck region, particularly in the transversospinal group, except for the semispinalis capitis muscle. All muscles were replaced by low density tissue or were atrophied at 30 years after disease onset. The gluteal group, the psoas major muscle, the lateral abdominal group and the levator scapulae muscle were preserved in the late stage. There were exceptional cases. In one patient, low density changes in the dorsal muscles in the neck region occurred at an early stage. In another patient, the quadriceps femoris muscles were more severely damaged than the hamstrings at 14 years of disease duration.

Serum CK levels

Although serum CK levels were very high, there was a tendency for levels to decrease with disease duration (figure 3). There was a trend in the distribution of the levels by

Table 1 Summary of dysferlin gene mutations of patients in this study

Patient	Sex	Age (years)	Disease duration (years)	Exon	Nucleotide change	Protein change	State
Dys48-1	M	54	23	28	c.2997G>T	p.Trp999Cys	Homozygous
Dys58-1	F	51	8	28	c.2997G>T	p.Trp999Cys	Homozygous
Dys64-1	M	58	19	28	c.2997G>T	p.Trp999Cys	Homozygous
Dys93-1	F	57	17	28	c.2997G>T	p.Trp999Cys	Homozygous
Dys99-1	F	55	11	28	c.2997G>T	p.Trp999Cys	Homozygous
Dys106-1	F	22	3	28	c.2997G>T	p.Trp999Cys	Homozygous
Dys113-1	M	57	17	28	c.2997G>T	p.Trp999Cys	Homozygous
Dys123-1	F	59	25	28	c.2997G>T	p.Trp999Cys	Homozygous
Dys133-1	M	66	8	28	c.2997G>T	p.Trp999Cys	Homozygous
Dys170-1	F	38	7	28	c.2997G>T	p.Trp999Cys	Homozygous
Dys13-1	M	43	29	28 34	c.2997G>T c.3771G>A	p.Trp999Cys p.Trp1257X	Compound heterozygous
Dys55-1	F	47	22	28 37	c.2997G>T c.3959_3960insA	p.Trp999Cys p.Met1320IlefsX26	Compound heterozygous
Dys114-1	M	50	15	Intron 25 28	c.2643+1G>A c.2997G>T	Splice site p.Trp999Cys	Compound heterozygous
Dys120-1	M	55	25	18 28	c.1566C>G c.2997G>T	p.Tyr522X p.Trp999Cys	Compound heterozygous
Dys124-1	F	36	12	18 28	c.1566C>G c.2997G>T	p.Tyr522X p.Trp999Cys	Compound heterozygous
Dys127-1	F	56	23	18 28	c.1566C>G c.2997G>T	p.Tyr522X p.Trp999Cys	Compound heterozygous
4	M	75	49	Intron 25 41	c.2643+1G>A c.4497delT	Splice site p.Phe1499LeufsX4	Compound heterozygous
5	M	Died at 59	Died at 42	21	c.1958delG	p.Gly653ValfsX3	Homozygous
15	F	50	34	37	c.3959_3960insA	p.Met1320IlefsX26	Homozygous
39	F	74	52	Intron 25	c.2643+1G>A	Splice site	Homozygous
44	M	41	14	29 41	c.3112C>T c.4497delT	p.Arg1038X p.Phe1499LeufsX4	Compound heterozygous
47	M	55	37	37	c.3959_3960insA	p.Met1320IlefsX26	Homozygous
Dys37-1	M	60	40	Intron 10	c.937+1G>A	Splice site	Homozygous
Dys37-2	F	51	24	Sister of Dys37-1			
Dys43-1	F	36	19	18	c.1566C>G	p.Tyr522X	Homozygous
Dys43-2	F	35	21	Sister of Dys43-1			
Dys46-1	F	67	48	41	c.4497delT	p.Phe1499LeufsX4	Homozygous
Dys50-2	M	70	29	41	c.4497delT	p.Phe1499LeufsX4	Homozygous
Dys59-1	F	49	27	28	c.2974T>C	p.Trp992Arg	Homozygous
Dys61-1	F	43	21	41	c.4497delT	p.Phe1499LeufsX4	Homozygous
Dys78-1	F	54	30	Intron 10	c.937+1G>A	Splice site	Homozygous
Dys84-1	F	64	45	14	c.1321C>T	p.Gln441X	Homozygous
Dys84-2	M	52	32	Brother of Dys84-1			
Dys89-1	F	68	40	18 28	c.1566C>G c.2974T>C	p.Tyr522X p.Trp992Arg	Compound heterozygous
Dys117-1	M	32	9	18	c.1566C>G	p.Tyr522X	Homozygous
Dys117-2	M	30	16	Brother of Dys117-1			
Dys126-1	M	23	2	Intron 4 54	c.342+1G>A c.6135G>A	Splice site p.Trp2045X	Compound heterozygous
Dys145-1	F	27	10	6	c.610C>T	p.Arg204X	Homozygous
Dys146-1	F	58	34	31 Intron 43	c.3373delG c.4794+1G>A	p.Glu1125LysfsX9 splice site	Compound heterozygous
Dys163-1	M	36	11	6	c.493delC	p.Leu165SerfsX48	Homozygous

c.2997G>T (p.Trp999Cys) mutation. Levels in the group homozygous for the c.2997G>T (p.Trp999Cys) mutation were lower than those of the other two groups.

Cardiac function

Although supine and standing position chest x-rays were mingled, in half of the patients the cardiothoracic ratio was >50%. No significant correlation was observed between EF and disease duration. Except for two patients, levels of EF were >50%. In all the patients, concentrations of atrial natriuretic peptide were within the normal range. Except for one patient, concentrations of brain natriuretic peptide were within the normal range. No significant correlation was observed between these peptides and disease duration. Although 19 patients

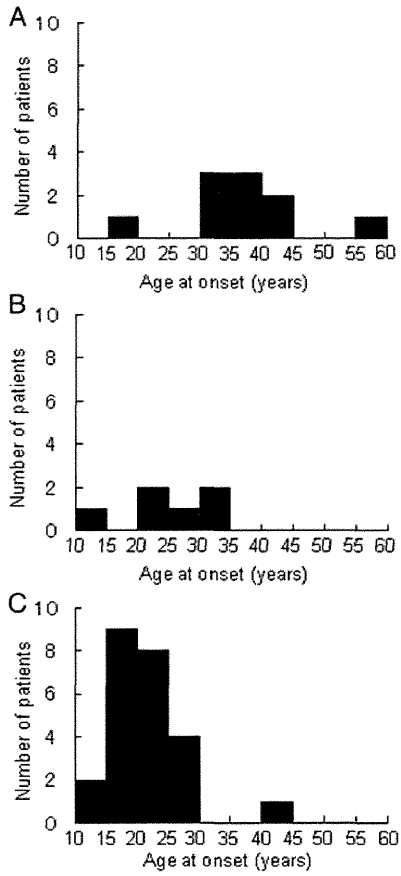

Figure 1 Histogram by age at onset. (A) Patients homozygous for the c.2997G>T mutation. (B) Patients heterozygous for the c.2997G>T mutation. (C) Patients without the c.2997G>T mutation.

exhibited normal findings on ECG, abnormalities were found in nine patients. The ECG showed premature ventricular contraction in one patient, one degree atrioventricular block in two patients, incomplete right bundle branch block in two patients, left axis deviation in two patients, left atrial hypertrophy in one patient, right ventricular hypertrophy in three patients, left ventricular hypertrophy in three patients, ST change in two patients and negative T in one patient.

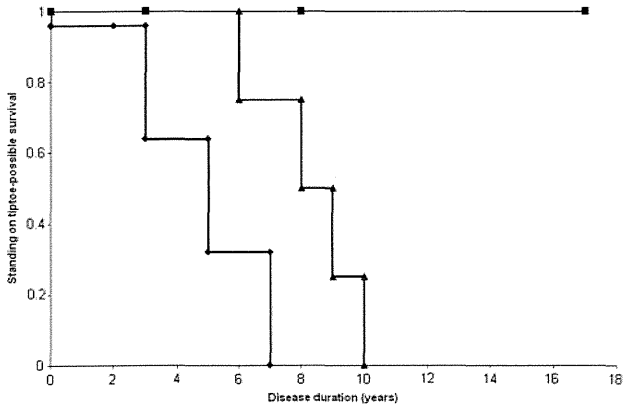

Figure 2 Standing on tiptoe—possible survival curve. Survival curve of patients homozygous for the c.2997G>T mutation (line with squares), those heterozygous for the c.2997G>T mutation (line with triangles) and those without the c.2997G>T mutations (line with diamonds).

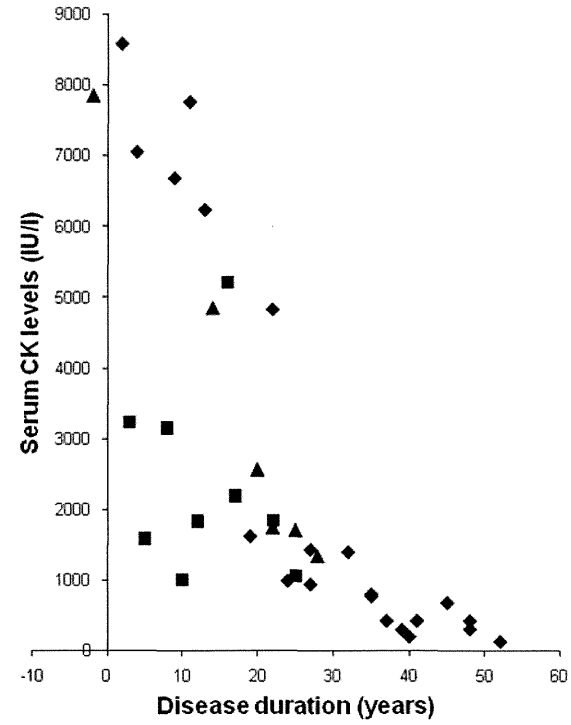

Figure 3 Serum creatine kinase (CK) levels during the disease course. Levels of serum CK in patients homozygous for the c.2997G>T mutation (squares), heterozygous for the c.2997G>T mutation (triangles) and those without the c.2997G>T mutations (diamonds).

Respiratory function

A statistically significant ($p<0.01$) correlation ($r=-0.545$) was observed between %VC and disease duration (figure 4). In 48% of patients, %VC was <80%. Although no significant correlation was observed between pCO_2 and disease duration, in 44% of patients, levels of pCO_2 were >45 mm Hg. In most patients, levels of pO_2 were >70 mm Hg. No significant correlation was observed between pO_2 and disease duration. Four patients had

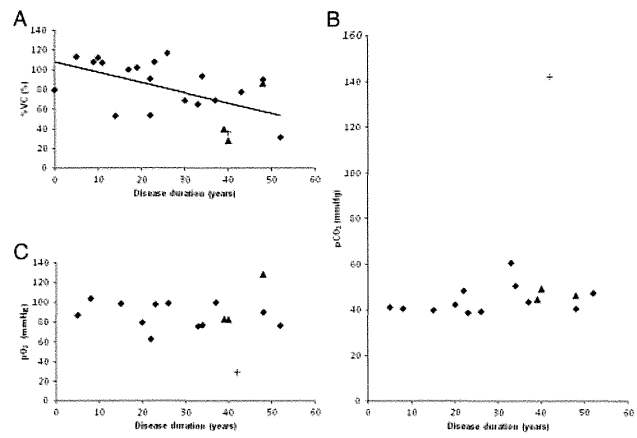

Figure 4 Respiratory function. (A) Per cent vital capacity (%VC) according to disease duration. The line is the regression line of %VC and disease duration. (B) Carbon dioxide partial pressure (pCO_2) according to disease duration. (C) Oxygen partial pressure (pO_2) according to disease duration. The triangles indicate levels in patients who had used non-invasive positive pressure ventilation. The cross (+) indicates the level in a patient who died after 42 years of disease duration of respiratory failure.